https://doi.org/10.5194/egusphere-2026-3584
Preprint. Discussion started: 30 June 2026
© Author(s) 2026. CC BY 4.0 License.

Satellite-based burned area reconstructions in land surface models: impacts on the land carbon cycle

Tim Stripp[1], Zhixuan Guo[2], Pierre Friedlingstein[1], Michael O'Sullivan[1], Stephen Sitch[1], Ana Bastos[3], Philippe Ciais[4], Jefferson Goncalves de Souza[1], Akihiko Ito[5], Wei Li[2], and Lei Ma[6]

[1]Faculty of Environment, Science and Economy, University of Exeter, Exeter, EX4 4QF, UK
[2]Department of Earth System Science, Ministry of Education Key Laboratory for Earth System Modeling, Institute for Global Change Studies, Tsinghua University, Beijing 100084, China
[3]Institute for Earth System Science and Remote Sensing, Leipzig University, Talstr. 35, 04103 Leipzig, Germany
[4]Laboratoire des Sciences du Climat et de l'Environnement, LSCE/IPSL, CEA-CNRS-UVSQ, Université Paris-Saclay, 91191 Gif-sur-Yvette, France
[5]Graduate School of Agricultural and Life Sciences, University of Tokyo, Tokyo, Japan
[6]Department of Geographical Sciences, University of Maryland, College Park, MD 20742, USA

Correspondence: Tim Stripp (ts857@exeter.ac.uk)

https://doi.org/10.5194/egusphere-2026-3584
Preprint. Discussion started: 30 June 2026
© Author(s) 2026. CC BY 4.0 License.

1 Abstract

Fire is a key Earth system process influencing vegetation distribution and the land carbon cycle, yet its representation within dynamic global vegetation (DGVM) models is generally poor, adding to the high level of inter-model uncertainty around simulated burned area (BA), fire emissions, and hence land carbon sink estimates. Here, we address this uncertainty by applying a satellite-based long-term reconstruction of burned area from 1901 to 2020 to five DGVM models, in order to assess the impacts of diagnostic BA on global carbon cycle estimates.

By diagnosing BA, we reduced the inter-model standard deviation in global fire emissions by 59% compared to the prognostic BA simulations, and significantly increased estimate agreement with observations spatially and regionally. We also moderately improved net land carbon sink estimates, reducing bias by 0.3 PgC year^{-1} against top-down constraints on average over 2001–2020, however the inter-model spread persisted. Additionally, regional simulated fire combustion rate (fire carbon emissions per unit BA) magnitudes and trends did not align with observations under diagnostic BA, influencing simulated land sink trends. This indicates poor representation of fire dynamics, specifically around the representation of fuel loads and combustion completeness, fire-induced mortality, fire intensity, and vegetation recovery processes.

We also explore land sink uncertainty associated with various diagnostic BA reconstructions using the JULES DGVM. By performing two JULES simulations using two reconstructed BA datasets derived from distinct satellite products (FireCCI5.1 and GFED5), we found a substantial difference in the land carbon sink (0.8 PgC year^{-1}) between the two simulations over 2001–2020. This shows that the underlying uncertainty in BA mapping and reconstructed BA trends can add a large source of uncertainty to modern day land sink estimates. Using a counterfactual simulation, we show that this uncertainty likely stems from differences in reconstructed pre-satellite era burned area dynamics leaving legacy impacts on both fire emission and ecosystem productivity estimates.

Our results show that although diagnostic burned area can greatly improve fire emission realism and constrain DGVMs, an enhanced representation of post-fire ecosystem impacts, fire intensity and fuel loads is needed in order to capture regional impacts of fire on the carbon cycle.

2 Introduction

Fire disturbance plays a crucial role within the Earth system, impacting vegetation composition and biomass, soil processes, atmospheric composition and climate (Bond et al., 2005; Bowman et al., 2009). Carbon emissions from fires are estimated to be between 2 and 4 PgC year^{-1} globally (equivalent to $\approx$ 20–40% of carbon emissions from fossil fuels in 2025, Friedlingstein et al., 2025a). However, much of this carbon flux from the land to the atmosphere is counteracted by post-fire regrowth, especially in grassland ecosystems where biomass lost through fire is generally fully recovered on short timescales (1–3 years, Parker et al., 2022; Gomes et al., 2020). In forest ecosystems, especially those that are not well adapted to fire (e.g. moist tropical forests such as those found in Amazonia), the level of fire-induced tree mortality may be high (Balch et al., 2011) and biomass may never be fully reaccumulated in many instances (Sato et al., 2016), leading to multi-decadal reductions to the global land sink (Silva et al., 2018, 2020). Additionally, in forest ecosystems prone to intense, severe fires (e.g. coniferous

https://doi.org/10.5194/egusphere-2026-3584
Preprint. Discussion started: 30 June 2026
© Author(s) 2026. CC BY 4.0 License.

boreal forests), fire-induced tree mortality and fire carbon emissions are also high (Webb et al., 2024) and forest recovery rates are slow (Palviainen et al., 2020), influencing the land carbon balance in these ecosystems (Xu et al., 2024).

Over time, humans have directly (e.g. cultivation and land-management practices) and indirectly (e.g. climate change) changed fire regimes globally, leading to changes in the global carbon cycle (Archibald et al., 2018). For example, over 1998–2015, burned area decreased globally by $\approx 25\%$, driven by agricultural expansion in savanna ecosystems (Andela et al., 2017). Further analyses support an increase in fire occurrence and intensity due to climate change in forest ecosystems (Zheng et al., 2021; Fan et al., 2022), especially in the extratropics (Jones et al., 2024), which has weakened the land carbon sink (Burton et al., 2024; Fan et al., 2022). This has led to near constant fire carbon emissions across the same period, despite the decline in burned area. Therefore, fire disturbances and fire regime changes play a fundamental role in controlling the size of the land carbon sink.

In carbon budgets like the Global Carbon Budget (GCB, Friedlingstein et al., 2025a), natural land sink estimates are obtained from dynamic global vegetation models (DGVMs), many of which are fire-enabled through the use of prognostic fire modules. These modules predict global burned areas based on ignition sources, climatic variables (e.g. temperature and precipitation), anthropogenic factors (e.g. GDP, land-use and population density) and simulated fuel loads. Fire emissions are then calculated based on BA, fuel loads, combustion completeness and emission factors, and post-fire impacts such as fire-induced mortality are applied. Since fire has such a strong influence on the land carbon sink, realistic fire representation within these models is vital to producing realistic land sink estimates. However, DGVM prognostic fire modules are generally poorly constrained leading to large variability in the burned area and fire emission estimates they produce both spatially and temporally, illustrated in FireMIP analyses (Hantson et al., 2020). In GCB, the DGVMs are also under-constrained and estimate global burned area between 0.6 $\text{Mkm}^2\ \text{year}^{-1}$ and 18.5 $\text{Mkm}^2\ \text{year}^{-1}$ in GCB 2024 (Friedlingstein et al., 2025b). Additionally, the majority of these prognostic fire models fail to reproduce the magnitude and direction of the observed negative trend in burned area across the beginning of the 21$^{\text{st}}$ century (Andela et al., 2017), and their ability to capture mega-fires associated with extreme weather conditions (which are increasing in frequency and can impact regional carbon balances, Cunningham et al., 2024; Walker et al., 2018) is limited. This disparity between fire representation across DGVMs adds to the uncertainty around land sink estimates, with land processes carrying the highest level of uncertainty in carbon budgets (Jones and Friedlingstein, 2020). On the other hand, satellite burned area products (several of which now exist) generally agree on burned area trends, seasonality, interannual variability and spatial patterns. Also, although some disparity is present around the magnitude of global total burned area, the range is far lower than that across DGVMs (ranging between $\approx 4\ \text{Mkm}^2\ \text{year}^{-1}$ and $\approx 8\ \text{Mkm}^2\ \text{year}^{-1}$ across products over 2001–2020). Therefore, diagnosing burned area from satellite products within DGVMs could greatly enhance DGVM fire realism and substantially increase burned area constraint across models, in turn reducing the uncertainty around fire carbon cycle impacts in these models.

However, most satellite burned area products only cover a short temporal range (with the majority covering from the late 1990s to the early 2020s), whereas the land carbon cycle has characteristic timescales from seconds (e.g. photosynthesis) through to decades and century (e.g. vegetation recovery and soil carbon dynamics). Thus, most DGVMs require to be spun-up to a pre-industrial state where equilibrium is reached prior to a transient simulation being performed, to quantify the human

https://doi.org/10.5194/egusphere-2026-3584
Preprint. Discussion started: 30 June 2026
© Author(s) 2026. CC BY 4.0 License.

impact on the carbon cycle. Therefore, in order to diagnose burned area in DGVMs, a burned area dataset spanning far into the past is needed. One workaround for this is to use a DGVM's prognostic fire model up to the starting point of a given satellite burned area dataset, and then switch to diagnostic burned area (diagnosed with this satellite product) (Poulter et al., 2015). The recent work of Ermitão et al., 2026 applied this method to a set of DGVMs, and found notable improvements to fire emission estimates compared to benchmarking datasets. However, the short nature of satellite burned area implies a switch from prognostic to diagnostic burned area in the 2000s that is far from ideal, since sudden changes to burned area (especially spatially) are likely to induce temporary trends in carbon cycle estimates. On the other hand, recent efforts have led to the creation of two satellite based reconstructed burned area datasets, detailed in Guo et al., 2025. These reconstructions, created using a machine learning (ML) algorithm trained on two satellite burned area products (FireCCI5.1, Chuvieco et al., 2019 and GFED5, Chen et al., 2023), provide global monthly burned areas between 1901 and 2020. Hence, applying these reconstructions as diagnostic burned area in DGVM simulations could allow for far more realistic long-term burned area representation across DGVMs while retaining or improving estimates of the modern day natural land sink.

In this study, we diagnose burned area from the satellite based burned area reconstructions from Guo et al., 2025 to DGVM models to assess the impacts of using long-term diagnostic burned area on carbon cycle estimates compared to prognostic burned area simulations. The FireCCI5.1 based reconstruction was applied to five DGVMs to assess how diagnostic BA impacts multi-model carbon cycle and natural land sink estimates, like those used in global carbon budgets. Specifically, we analyse how both fire emission and land sink estimates differ between simulations and how these compare to benchmarking datasets. Additionally, we applied two distinct reconstructions to a single DGVM, the JULES DGVM (Best et al., 2011; Clark et al., 2011; Burton et al., 2019), in order to assess the level of uncertainty around how differences between reconstructions may impact carbon cycle estimates.

3 Materials and methods

3.1 Burned area products

For diagnostic burned area data in our simulations, the two aforementioned ML based burned area reconstructions were used (Guo et al., 2025), constructed based on the satellite burned area products FireCCI5.1 (Chuvieco et al., 2019) and GFED5 (Chen et al., 2023). To create these reconstructions, a ML model was trained on burned area data between 2003 and 2020, and then data on 16 explanatory variables (consisting of observations, other reconstructed datasets and model outputs) were used to extend burned area estimates into the past. The long-term trends and absolute burned area values differ noticeably between these two reconstructions (global burned area is on average 2 Mkm^2 higher across the entire GFED5 reconstruction than the FireCCI5.1 reconstruction, Fig. 1). This discrepancy is to be expected since GFED5 uses medium-resolution (tens of metres) burned area products to better constrain omission and commission error estimates, particularly the omission of small fires missed by coarse-resolution (hundreds of metres) satellite sensors (Randerson et al., 2012; Chen et al., 2023). As a result, global burned area estimates are notably higher in GFED5 compared to its counterparts, but these estimates may be more reliable due to the increased agreement with medium-resolution products which exhibit fewer omission and commission errors.

https://doi.org/10.5194/egusphere-2026-3584
Preprint. Discussion started: 30 June 2026
© Author(s) 2026. CC BY 4.0 License.

In terms of long-term burned area dynamics, the FireCCI5.1 reconstruction global total burned area decreases from 1901 to 1978, then increases up to 2008, followed by a decrease between 2008 and 2020 (based on breakpoint analysis). In contrast, the GFED5 reconstruction does not exhibit a negative trend initially (due to no negative trend in Southern Hemisphere Africa), but contains a positive trend from 1979 to 2003, after which burned area decreases. Despite these differences in long-term trends, the interannual variability between the two reconstructed BA datasets is moderately correlated globally ($R^2 = 0.58$ over the reconstructed period: 1901–2002), suggesting broad agreement on the timing of historical extreme fire years.

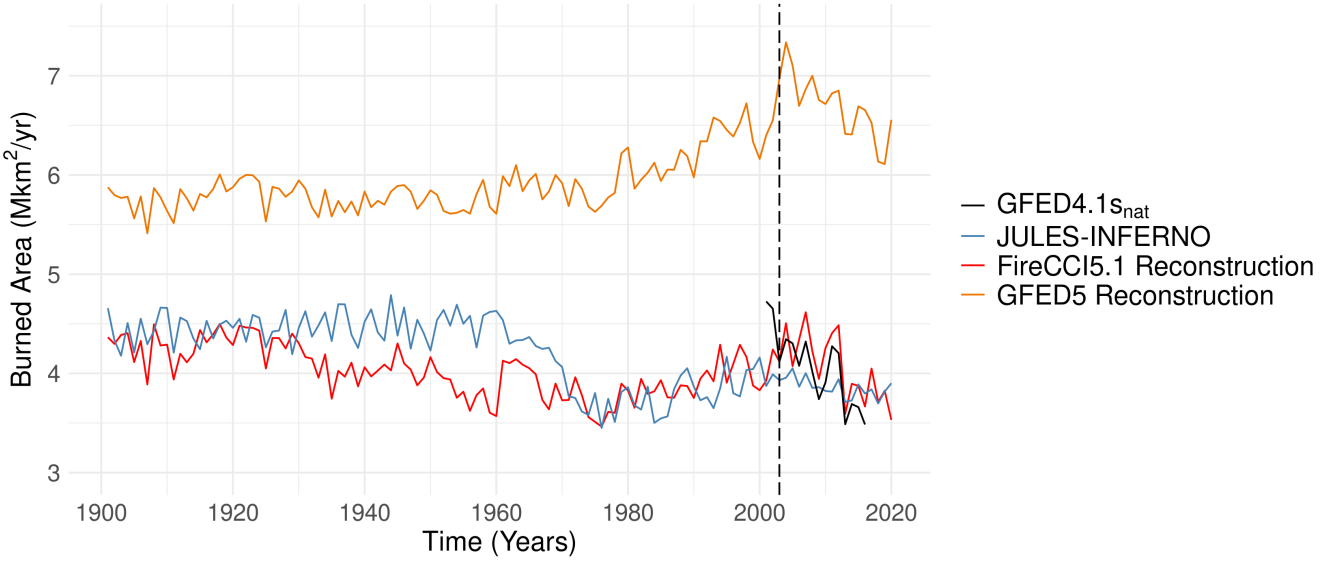

Figure 1. Global total burned area time series for the two reconstructed burned area datasets used in the diagnostic BA JULES simulations (described in Section 3.1, Guo et al., 2025), with global total prognostic burned area from the JULES-INFERNO fire model also shown. The dashed black line indicates the start point of the training data used by the ML model (2003), and the GFED4.1s "natural" burned area data (with land-use associated fires removed) over 2001–2016 is shown in black.

3.2 Model simulations

Model simulations listed in Table 1 were used to assess the impacts of diagnostic burned area on DGVM carbon cycle estimates. Specifically, comparisons between PS and DS_{CCI} were used to assess the impact of diagnostic burned area compared to prognostic on modern day carbon cycle estimates across several DGVMs (shown in Table 2), whilst comparisons between DS_{CCI} and DS_{GFED} were used to assess the level of uncertainty differing burned area reconstructions have on modern day carbon cycle estimates (in the JULES model). Also, we performed an additional counterfactual JULES simulation based on the DS_{CCI} simulation (DS_{CCI} CF) to isolate the impact of BA dynamics on JULES carbon cycle estimates. Specifically, in this counterfactual simulation the mean monthly burned area from 1969–1978 was repeated for each year from 1979 to 2008, to

https://doi.org/10.5194/egusphere-2026-3584
Preprint. Discussion started: 30 June 2026
© Author(s) 2026. CC BY 4.0 License.

assess how the rise in global burned area between 1979 and 2008 present in the FireCCI5.1 reconstruction affected the JULES DS_{CCI} land sink estimate. More broadly, this counterfactual is used to assess the influence of BA dynamics on fire emission and ecosystem productivity estimates over time.

Simulation	BA Type	BA Source	Models Involved
PS	Prognostic	DGVM fire model	All participating DGVMs
DS_{CCI}	Diagnostic	FireCCI5.1 reconstruction	All participating DGVMs
DS_{GFED}	Diagnostic	GFED5 reconstruction	JULES only
DS_{CCI} CF	Diagnostic	FireCCI5.1 reconstruction (average of 1969–1978 repeated post 1978)	JULES only

Table 1. Table describing model simulations used to compare prognostic and diagnostic fire in land surface model simulations. The DS_{GFED} and DS_{CCI} CF simulations were only carried out by the JULES DGVM to assess uncertainties around land sink estimates under differing diagnostic BA data (see Section 4.2).

These simulations are either directly from or are adaptations of those found in the TRENDY protocol for the Global Carbon Budget 2024 (Sitch et al., 2024). In all simulations, both atmospheric CO_2 concentration and climate are forced, meaning the effects of climate change and carbon fertilisation are accounted for. Additionally, land-use was fixed at pre-industrial levels (the year 1700 from LUH2, Hurtt et al., 2011) and the CRU-JRA2.5 climatological forcing data was used (Harris et al., 2020; Kobayashi et al., 2015), which covers 1901–2024. Model spin-up also followed the TRENDY project protocol, with atmospheric CO_2 and land-use fixed at pre-industrial levels, and with climate data from the years 1901–1920 either recycled or randomly sampled until model pools reached equilibrium. During the spin-up of the diagnostic burned area simulations, the 1901–1920 reconstructed BA was recycled in four of the five participating models, and randomly sampled in the OCN model.

In the diagnostic BA simulations, burned area was supplied to all DGVMs in a similar manner, with a constant proportion of burned area being supplied to each PFT in each grid-cell. Although, the JULES model split burned area across all PFTs, whilst the other four models only supplied burned area to natural PFTs.

The PS simulation is identical to the TRENDY "S2" simulation, used in the GCB as an estimate of the natural land sink (the net uptake of carbon by the land, excluding any land-use change emissions). Since fire is used as tool for land-use change in many instances and many fires are associated with modern day land-use and land management (Aragão et al., 2018), diagnostic burned area needs careful inclusion in DGVMs in order for the DS_{CCI} and DS_{GFED} simulations to be equivalent to PS (i.e. with all land-use change emissions excluded). For this reason, the ML model used for the reconstructions was trained on BA products with land-use associated fires removed. Specifically, BA in cropland and cropland mosaic land cover in ESA CCI Land Cover (ESA, 2017) was removed from FireCCI5.1 prior to training, whilst BA from peat fires, agriculture fires, and tropical deforestation and degradation fires was removed from GFED5. This means the reconstructions are corrected for land-use associated fires in theory.

https://doi.org/10.5194/egusphere-2026-3584
Preprint. Discussion started: 30 June 2026
© Author(s) 2026. CC BY 4.0 License.

In the prognostic BA simulation, BA was calculated by each of the participating DGVM's prognostic fire module. These modules, along with information on how fire carbon cycle impacts are calculated in each model (e.g. fire emissions, fire-induced mortality) are described in Table 2.

3.3 Benchmark datasets and analysis metrics

To analyse the impact of diagnostic burned area versus prognostic on DGVM carbon cycle estimates, the following benchmark datasets were used. Firstly, to assess fire emission estimate accuracy, the GFED4.1s (van der Werf et al., 2017) and GFED5 (Werf et al., 2025) fire emission products were used. Both GFED4.1s and GFED5 use a bottom-up approach to estimate fire emissions. Specifically, satellite burned areas from MODIS (Giglio et al., 2016) are modified to account for commission and omission errors (mainly the omission of small fires). Then, a carbon cycle model (CASA, Potter et al., 1993) is used to estimate fuel loads, which are combined with field measurement constrained fuel consumption maps to estimate fire emissions. This approach means fire emission estimates are constrained based on both burned area and fuel consumption observations, leading to close alignment with atmospheric observations (Werf et al., 2025). Therefore, these products were deemed suitable to use as benchmarks in this study. In the newer GFED5 product, enhancements are made, with the main difference being the use of medium-resolution burned area products to better constrain omission and commission error estimates. This leads to a 61% higher global burned area and 65% higher global fire emissions in the GFED5 product compared to GFED4.1s (Werf et al., 2025). However, most other widely used global burned area products (including the FireCCI5.1 product used in the Multi-Model diagnostic BA simulations) estimate a similar global burned area to the GFED4.1s product (Fig. 1), meaning we use GFED4.1s and GFED5 as emission benchmarks in this study since burned area and fire emissions are highly correlated.

We derived the "natural" fire emissions from these products by removing all land-use associated fire emissions (emissions from peat fires, tropical deforestation and degradation fires and agricultural fires removed, aligning with the burned area reconstructions). Emission partitions across land cover classes were only available for the years 2001–2016 in GFED4.1s, and 2002-2020 in GFED5, meaning the products over the shared timespan (2002–2016) were used as our fire emission benchmarks. The FireCCI5.1 and GFED4.1s burned area is similar, meaning this dataset was used primarily when assessing the realism of DS_{CCI} fire emission estimates spatially. On the other hand, the GFED5 "natural" burned area and DS_{GFED} burned area is almost identical, meaning DS_{GFED} fire emission estimates are directly comparable to GFED5 "natural" emission estimates. Also, to assess fire combustion rate (fire emissions per unit burned area), both the GFED4.1s and GFED5 products were used. However, the GFED4.1s product does not provide burned area partitions, meaning the average of the GFED5 partitions over 2002–2016 were used to augment the GFED4.1s BA.

To assess changes to land sink estimates we used the GCB residual sink and the 14 atmospheric inversions used in the GCB (Luijkx et al., 2024), adjusted for the lateral river flux and land-use change emissions (as to be equivalent to DGVM natural land sink estimates). To perform this adjustment, the river flux is based on (Lacroix et al., 2024), applied equally annually, while land-use change emission estimates come from the four bookkeeping (BK) models used in GCB (BLUE, Hansis et al., 2015; OSCAR, Gasser et al., 2020; H&C, Houghton and Castanho, 2023; LUCE, Qin et al., 2024). To calculate uncertainty around the ensemble means, the inter-ensemble standard deviation of the inversions and land-use change emission BK models

DGVM Name	Dynamic Vegetation?	Prognostic Fire Model	Available Fuel	Fire Emissions	Combustion Completeness	Fire-induced Mortality	Fire Intensity Calculated? Impact on Emissions/Mortality
JULES (Best et al., 2011; Clark et al., 2011)	Yes	JULES-INFERNO (Mangeon et al., 2016; Burton et al., 2019)	Available fuel loads are based on 'litter' pools (dpm, rpm), with live vegetation indirectly contributing through mortality	Fire emissions are calculated as 'litter' fuel load inputs scaled with combustion completeness (CC), plus a constant percentage of vegetation carbon killed by fire (13%)	CC values scale linearly between minima and maxima in each 'litter' pool with soil moisture in the top 10cm of soil	Constant percentages of PFT biomass are removed for a given burned area as vegetation carbon killed by fire (40% in forest PFTs, 100% in grasses and 60% in shrubs), PFT fractional coverage is not directly impacted by fire	No
EDv3 (Moorcroft et al., 2001; Ma et al., 2022)	Yes	EDv3 (Moorcroft et al., 2001; Ma et al., 2022)	Available fuel loads are based on the total aboveground biomass of live vegetation across all patches	Fire emissions are calculated as fuel loads scaled by combustion completeness constants and survivorship of each individual cohort	CC is assumed of constant value	Survivorship is height dependent. For grass PFTs, survivorship is assumed to be 0. For tree PFTs, survivorship is set to 0.3 when canopy height is below a 20 m threshold and 0.8 when canopy height exceeds this threshold	No
ORCHIDEE (Krinner et al., 2005; Guimberteau et al., 2018)	No	ORCHIDEE-MICT-SPITFIRE (Yue et al., 2014; Thonicke et al., 2010)	Fuel loads are accumulated by background mortality of biomass, senescence-driven turnover of leaves and roots, and live grass biomass	Fire emissions are calculated as the product of burned area fraction, fuel loads, combustion completeness and trace gas emission factors	CC values are linearly determined completely by live/dead fuel wetness. Fuel wetness is unitless, ranging in 0-1. The linear relationship varied across different ranges of wetness	For forest PFTs, fire-induced mortality consists of crown damaged induced mortality and cambial damage induced mortality. For non-forest PFTs, fire-induced mortality is not applied	Yes, fire intensity directly impact scorched height for trees, further influencing proportion of crown damage and tree mortality. Fire intensity would not impact emissions.
VISIT-UT	No	(Thonicke et al., 2001)	Litter and plant stem simulated by VISIT-UT carbon cycle scheme	Burned area · fuel load · burned fraction · emission factor (Akagi et al., 2011)	Implicitly fixed by biome-specific burned fraction (Hoelzemann et al., 2004)	Burned biomass was removed from the carbon pools. Individual mortality was not explicitly considered	Implicitly fixed by biome-specific burned fraction (Hoelzemann et al., 2004)
OCN (Zaehle et al., 2010)	No	Glob-FIRM (Thonicke et al., 2001)	Available fuel is calculated based on aboveground litter, except woody litter. Fire is calculated for natural PFTs only.	Fire emissions are calculated based on burned area per PFT, which is modified based on PFT resistance parameters, multiplied by the available biomass in the different pools and pool-specific combustion completeness (CC).	CC depends on the biomass pools and only applies to aboveground components.	Burned biomass is removed from the carbon pools. PFT fractional coverage is not directly impacted by fire.	Fire intensity not explicitly calculated, but no fire can occur if litter load is too low, or litter moisture too high.

Table 2. Table describing TRENDY models participating in diagnostic burned area simulations.

https://doi.org/10.5194/egusphere-2026-3584
Preprint. Discussion started: 30 June 2026
© Author(s) 2026. CC BY 4.0 License.

https://doi.org/10.5194/egusphere-2026-3584
Preprint. Discussion started: 30 June 2026
© Author(s) 2026. CC BY 4.0 License.

were combined, and minimum and maximum estimates were obtained through testing all combinations of the inversion and land-use ensembles. Of these 14 inversion datasets, eight fully cover the period 2001–2020, so these are used in our analysis of this period. These eight inversions, and the four land-use change emission BK model estimates over the same period, can be seen in Fig. S4.

We define the DGVM net land sink (excluding land-use change) as Net Biome Production (NBP) estimates, calculated as:

$$\mathrm{NBP} = \mathrm{NPP} - \mathrm{HR} - \mathrm{fFire} - \mathrm{fHarvest}, \tag{1}$$

where NPP denotes Net Primary Productivity, HR denotes Heterotrophic Respiration, fFire denotes the fire emission carbon flux and fHarvest denotes the harvest emission carbon flux (excluding wood product emissions). Net Ecosystem Production (NEP) is also investigated, defined as NPP − HR.

The following metrics were used to compare fire emission and land sink estimates to the observational datasets listed previously. Firstly, mean bias over the relevant period was used to assess the absolute prediction accuracy of each model regionally, based on values integrated over all grid cells within each region. Temporal trends were assessed based on least squares regression models on each regional annual time series (along with 95% confidence intervals). Meanwhile, for spatial accuracy assessments the normalised mean error (NME) score was used, calculated across all land grid cells (adjusted for grid cell size) as:

$$\mathrm{NME} = \frac{\sum_i A_i \cdot (|y_i - x_i|)}{\sum_i A_i \cdot (|x_i - \bar{x}|)}, \tag{2}$$

where, for grid cell i, A_i denotes the cell area, y_i and x_i denote the modelled and benchmark value (respectively, averaged over the relevant time period), and $\bar{x}$ denotes the mean observed value across all cells. Finally, we use inter-model standard deviation as an indicator of inter-model uncertainty, later referred to as the 'inter-model spread'. For regional analyses, the 14 GFED regions were used (Werf et al., 2025), shown in Fig. S1.

4 Results

4.1 Diagnostic burned area across multiple models

4.1.1 Fire emissions

When diagnosing BA across the five DGVM models (JULES, EDv3, VISIT-UT, ORCHIDEE and OCN), improvements to global fire emissions (fFire) were made. Specifically, we reduced the inter-model spread by 59% (1.8 PgC year^{-1} to 0.7 PgC year^{-1}) and aligned well with GFED4.1s "natural" mean emissions (where global total burned area is similar, Fig. 1). Global emission trends varied between benchmark datasets (weak but significant negative trend in GFED4.1s, non-significant trend in GFED5) due to differences in burned area trends. Therefore, we focus on trends in fire combustion rates (fFire per unit BA, Section 4.1.2), which better isolate combustion processes.

https://doi.org/10.5194/egusphere-2026-3584
Preprint. Discussion started: 30 June 2026
© Author(s) 2026. CC BY 4.0 License.

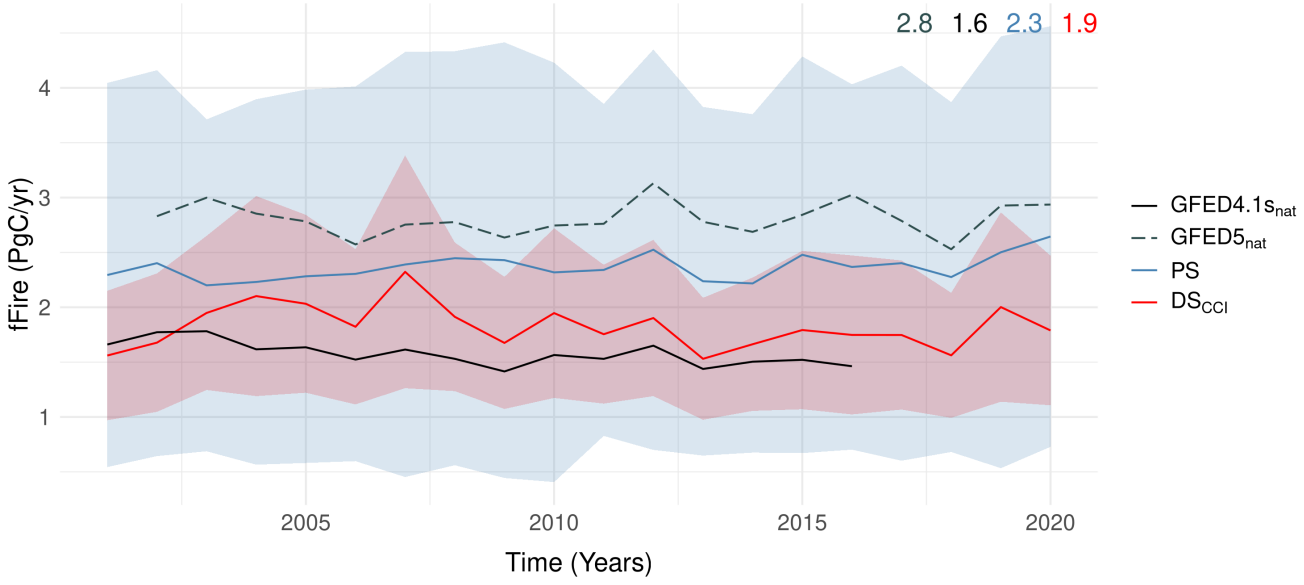

Figure 2. Multi-model mean and GFED "natural" global fire emission estimates, with ribbons showing inter-model spread in each simulation. Numbers in the top right show GFED and multi-model averages over the GFED shared period (2002–2016).

Spatially and regionally, further improvements to emission estimates were observed when diagnostic burned area was applied (Fig. 3, Table S1). In African savanna regions (which account for the majority of global fire emissions and BA), fire emissions and BA were generally underestimated in the prognostic simulations compared to observation-based estimates. When burned areas were diagnosed, this bias was reduced substantially, with close alignment in these regions with the GFED4.1s "natural" fire emission product on average (where BA is similar) and improved agreement with the GFED5 "natural" product (where BA is notably higher). Furthermore, in Europe, parts of Central and Southern Asia, North America and the Middle East prognostic fire models produced highly variable fire emissions and BA estimates that were higher than observations on average. Therefore, under diagnostic BA biases and inter-model spread were also reduced in these regions (Fig. 3, Table S1). However, despite similar burned area to the GFED4.1s "natural" product, fire emissions remained generally overestimated in South America and underestimated in boreal regions, even under diagnostic BA. These patterns were particularly prevalent along the arc of deforestation in Southern Amazonia and the Cerrado, and in boreal forested areas of Siberia and Northern Canada and Alaska.

Spatial improvements to fire emission estimates under diagnostic BA are further illustrated by the substantially reduced NME values between DGVM estimates and GFED4.1s and GFED5 (observed in all models except EDv3, Table 3).

https://doi.org/10.5194/egusphere-2026-3584
Preprint. Discussion started: 30 June 2026
© Author(s) 2026. CC BY 4.0 License.

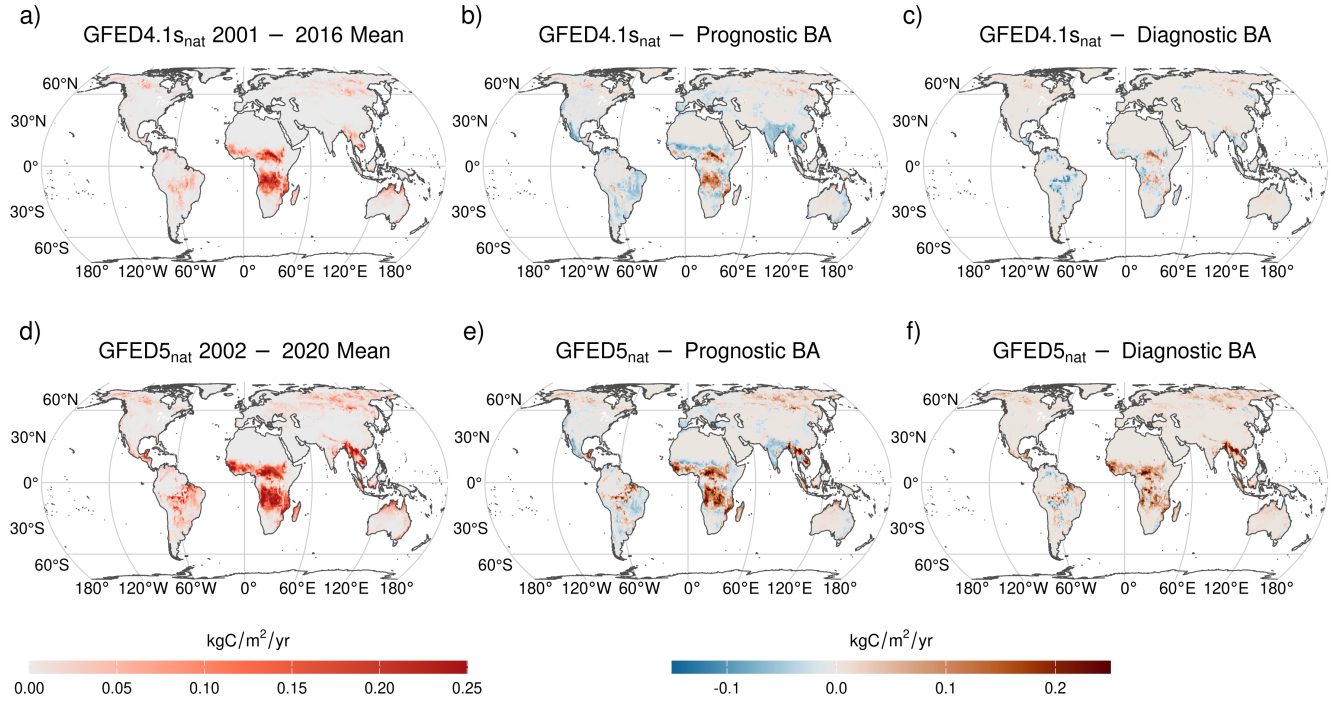

Figure 3. Spatial plots of GFED4.1s and GFED5 "natural" fire emission estimates globally (panels a and d), and differences between these and multi-model average emissions under prognostic and diagnostic BA (panels b, c, e and f). For GFED4.1s the data was averaged over 2001–2016 (panels a–c), while the average across 2002–2020 was used for GFED5 (panels d–f).

		Spatial Performance (Normalised Mean Error)				
Benchmark	Simulation	JULES	EDv3	VISIT-UT	ORCHIDEE	OCN
GFED4.1s$_{nat}$	PS	0.94	0.82	1.27	1.03	2.02
	DS$_{CCI}$	0.50	0.88	0.48	0.40	0.91
GFED5$_{nat}$	PS	0.73	0.80	0.96	0.79	1.01
	DS$_{CCI}$	0.50	0.73	0.57	0.55	0.54

Table 3. Spatial NME values of DGVM fire emissions against the GFED4.1s and GFED5 "natural" products under prognostic (PS) and diagnostic (DS$_{CCI}$) burned areas, calculated across all land grid cells. Coloured highlighting represents performance: green (NME $\leq$ 0.6, good), yellow (0.6 $<$ NME $\leq$ 0.8, moderate), orange (0.8 $<$ NME $\leq$ 1.0, poor), and red (NME $>$ 1.0, very poor).

https://doi.org/10.5194/egusphere-2026-3584
Preprint. Discussion started: 30 June 2026
© Author(s) 2026. CC BY 4.0 License.

4.1.2 Fire combustion rates

Our new DS_{CCI} simulations retained good agreement with GFED "natural" estimates of fire combustion rate (fire emissions per unit burned area) on average globally, but inter-model spread (S.D) was not reduced (Fig. 4), with model means ranging from 0.3 kgC m^{-2} $year^{-1}$ to 0.7 kgC m^{-2} $year^{-1}$ under diagnostic BA.

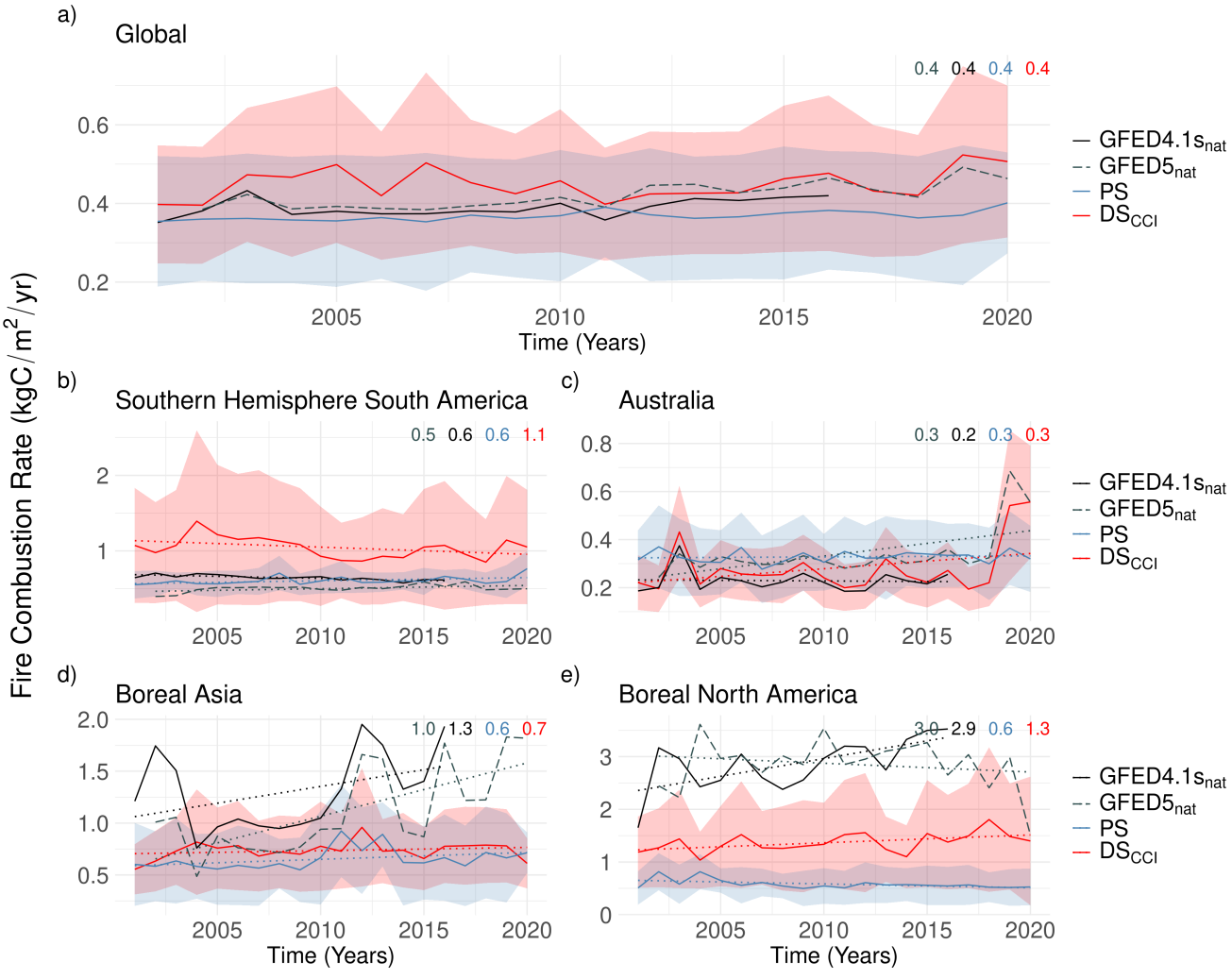

Figure 4. Multi-model mean and GFED "natural" fire combustion rate estimates globally, with ribbons showing inter-model spread in each simulation (panel a). Panels b–e show estimates and inter-model spread in four high fire GFED regions (Fig. S1). Numbers in the top right of each panel show GFED "natural" and multi-model averages over the whole time span.

Surprisingly, the satellite-constrained model simulations did not capture the significant positive trend in global fire combustion rate present in GFED4.1s and GFED5 of 0.7 % $year^{-1}$ and 1.2 % $year^{-1}$, respectively. Across models, simulated global

https://doi.org/10.5194/egusphere-2026-3584
Preprint. Discussion started: 30 June 2026
© Author(s) 2026. CC BY 4.0 License.

trends were non-significant, with a weak positive trend of 0.1 % year^{-1} on average. In GFED4.1s and GFED5, this positive trend mainly stems from Northern Hemisphere Africa and Boreal Asia (Fig. 4, Table S3). In Northern Hemisphere Africa this trend was replicated by some models, with ORCHIDEE and OCN producing significant trends of similar magnitude to those in GFED (Table S3). On the other hand, in Boreal Asia, whilst VISIT-UT, ORCHIDEE and OCN exhibited significant positive trends, these trends were sensitive to the time period and substantially weaker than GFED "natural" product trends (Fig. 4, Table S3).

The magnitudes of fire combustion rates also aligned poorly regionally with the GFED "natural" products, with a high level of inter-model spread present in many regions under diagnostic BA (Fig. 4, Table S2). In boreal regions, our modelled fire combustion rates fell far short of GFED on average, particularly in Boreal North America where, even though increased compared to prognostic simulations, rates were more than a factor of 2 lower than both GFED4.1s and GFED5 under diagnostic BA. Contrastingly, in moist tropical regions (South and Central America, South East and Equatorial Asia) fire combustion rates were greater than GFED on average, and inter-model spread was high (Fig. 4, Table S2).

In many regions (e.g. South and Central America, Boreal North America), inter-model spread was notably higher under diagnostic BA compared to prognostic (Table S2), despite burning being spatially consistent in these simulations.

Interestingly, under diagnostic burned area models were able to simulate the sudden increase in fire combustion rate in Australia in the years 2019 and 2020 (Fig. 4c), associated with the "Black Summer" extreme fire event (Ahmed and Ledger, 2023; Udy et al., 2024).

4.1.3 Land sink estimates

Diagnosing BA reduced the multi-model mean land sink by 0.3 ± 0.4 PgC year^{-1} over 2001–2020 compared to the prognostic simulations, despite the concurrent reduction in fire emissions. The DGVMs now better align with top-down constraints from atmospheric inversions (adjusted for land-use change emissions and the river flux) and the GCB residual sink on average over this period, although the model ensemble performed well globally under both prognostic and diagnostic burned areas (Fig. 5). The majority of the reduction to the land sink is attributable to the JULES, EDv3 and OCN models (which reported sink reductions of 0.9 PgC year^{-1}, 0.6 PgC year^{-1} and 0.5 PgC year^{-1} respectively) while the ORCHIDEE and VISIT-UT models both reported a slight increase in sink size (< 0.1 PgC year^{-1} on average).

The regions which contributed the most to the global reduction in the land sink were Southern Hemisphere Africa, South America, and Boreal Asia (Table S4). In the case of Southern Hemisphere Africa and South America these reductions brought estimates more in line with the mean of the adjusted inversion datasets, although land sink estimates lay within ± 1 S.D of the inversions on average in both these regions under both diagnostic and prognostic BA. On the other hand, in Boreal Asia the reduction in sink size moved the land sink estimate farther from the average of the inversions.

Across 2001–2020, three of the five models exhibited significant positive trends in NBP under diagnostic burned area (JULES, EDv3 and OCN, Fig. S2). In JULES and OCN, the trend in the prognostic BA simulation was non-significant, while EDv3 exhibited a significant positive trend under prognostic BA, but of a lower magnitude than that of the diagnostic BA simulation. By comparing trends in NBP plus fire emissions (equivalent to net ecosystem production minus harvest emis-

https://doi.org/10.5194/egusphere-2026-3584
Preprint. Discussion started: 30 June 2026
© Author(s) 2026. CC BY 4.0 License.

sions) between simulations with prognostic and diagnostic BA, we can isolate the influence of fire emission trends on NBP trends. Using this approach, trends in NBP plus fire emissions are similar between diagnostic and prognostic BA simulations in all models except JULES (Fig. S2). This suggests that the stronger positive NBP trends under diagnostic BA were largely attributable to modelled negative trends in global fire emissions, except in JULES, where burned area trends may have notable impacts on the carbon cycle (discussed in Section 4.2).

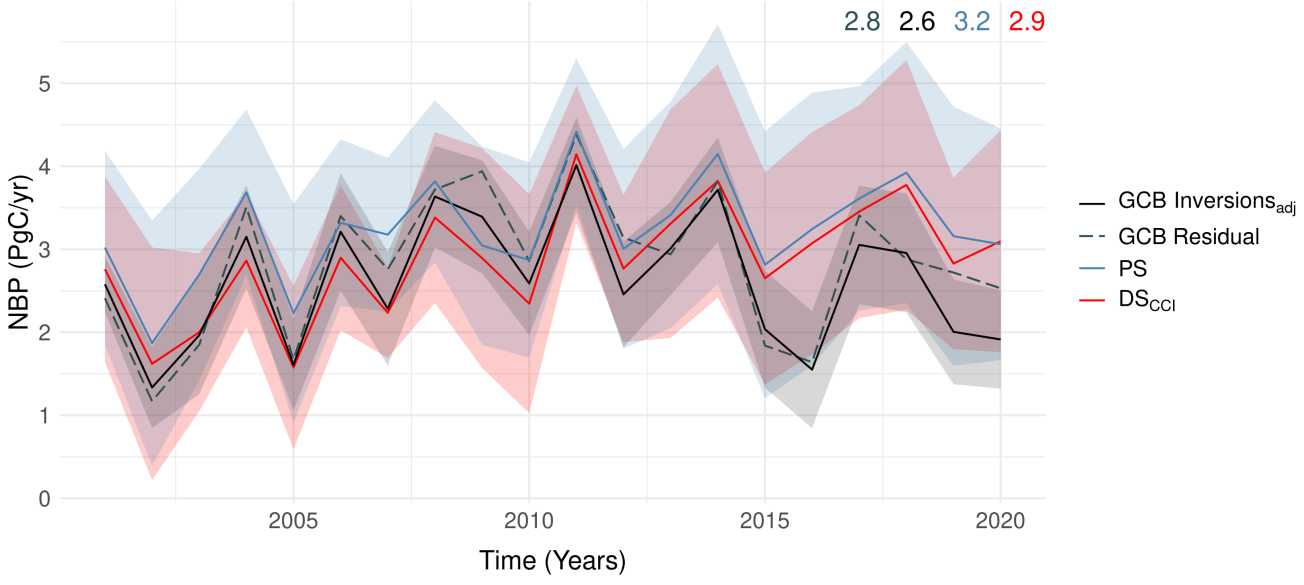

Figure 5. Multi-model mean and observational global land sink estimates, with ribbons showing inter-model spread in each simulation and the uncertainty in the GCB inversions (1 S.D) arising from the combination of multiple inversion products and GCB land-use change datasets. Numbers in the top right show GCB inversion$_{adj}$, GCB residual, and multi-model averages over the 2001–2020 period. Here, GCB inversion$_{adj}$ denotes the GCB inversion datasets adjusted for land-use change emissions and the river flux (described in Section 3.3).

4.2 JULES burned area sensitivity experiment

Since notable differences in both global total burned area and burned area dynamics are present between the two burned area reconstructions produced by Guo et al., 2025 (Section 3.1, Fig. 1), we performed a second simulation in the JULES DGVM with the GFED5 based reconstruction to assess the impact of these differences on carbon cycle estimates.

4.2.1 Fire emissions and land sink estimates

By applying the two distinct BA reconstructions to JULES, we found that fire emission estimates scaled well globally, with very similar average total emissions between GFED5 “natural” emissions and the diagnostic simulation with GFED5 BA, and

https://doi.org/10.5194/egusphere-2026-3584
Preprint. Discussion started: 30 June 2026
© Author(s) 2026. CC BY 4.0 License.

reasonable agreement between GFED4.1s "natural" emissions and the diagnostic simulation with FireCCI5.1 BA (Fig. 6b). Similar regional and spatial improvements to those seen in the multi-model analysis were also present.

Surprisingly, modern day land sink estimates varied substantially between simulations. Specifically, over 2001–2020 NBP was 2.7 PgC year^{-1} in the prognostic simulation, 1.8 PgC year^{-1} in the diagnostic simulation with FireCCI5.1 BA and 1.0 PgC year^{-1} in the diagnostic simulation with GFED5 BA. This NBP estimate in the simulation with GFED5 diagnostic BA fell below all GCB inversion and land-use dataset change combinations (minimum of 1.2 PgC year^{-1}).

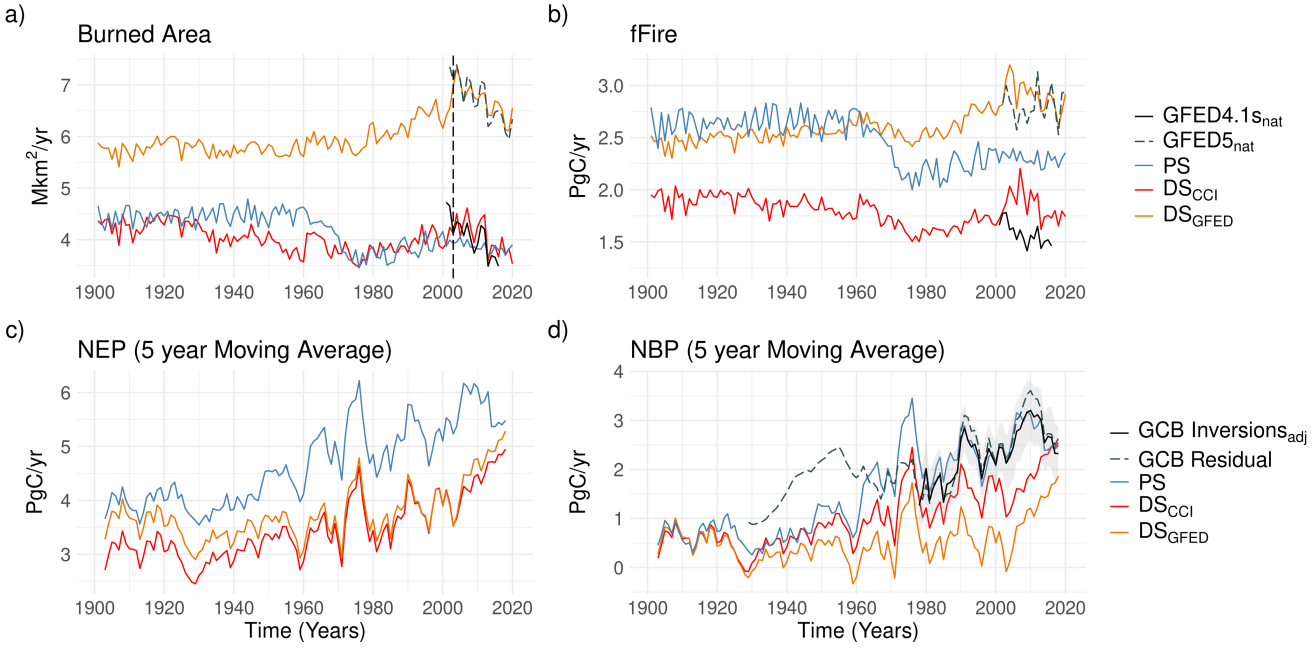

Figure 6. Global BA, fire emissions, NEP, and NBP estimates in the JULES prognostic and diagnostic BA simulations. The black dashed vertical line in panel a shows the start of the training period. GFED4.1s and GFED5 "natural" BA and fire emissions are shown in panels a and b, respectively, while GCB inversions (adjusted for land-use change emissions and the river flux) and the GCB residual are shown in panel d. The grey ribbon shows uncertainty (1 S.D) in the GCB inversions arising from the combination of multiple inversion products and GCB land-use change datasets.

4.2.2 Burned area dynamics and JULES land sink estimates

Historically, between 1901 and the mid 1970s, BA decreased in the FireCCI5.1 reconstruction but increased slightly in the GFED5 reconstruction. This difference in burned area dynamics coincides with a divergence in fire emissions and convergence in NEP between the two simulations, leading to divergence in NBP (Fig. 6). Also, in the prognostic BA simulation a significant drop in BA occurs in the 1960s, coinciding with divergence between the NBP in this simulation and the diagnostic simulations. Between the late 1970s and the early 2000s a rise in burned area occurs in both reconstructions, with this rise being of

https://doi.org/10.5194/egusphere-2026-3584
Preprint. Discussion started: 30 June 2026
© Author(s) 2026. CC BY 4.0 License.

higher magnitude in the GFED5 reconstruction. This coincides with further divergence between the diagnostic and prognostic simulation NBP.

The fact that divergence in NBP between the simulations is linked to differences in burned area dynamics specifically suggests that these dynamics influence JULES NBP estimates (through changes to both fire emissions and NEP), rather than the baseline level of BA. To evidence this further, we performed an additional counterfactual JULES simulation based on the DS_{CCI} simulation, described in Section 3.2, Table 1.

4.2.3 FireCCI5.1 1979–2008 burned area dynamics impact

Based on our counterfactual simulation, DS_{CCI} CF, the rise in burned area between 1979 and 2008 in the FireCCI5.1 reconstruction led to a substantial drop in the JULES natural land sink of 0.4 PgC year^{-1} on average, with the increase in fire emissions only accounting for $\approx 30\%$ of this decrease and the decrease in net ecosystem production (NEP = NPP - HR) accounting for the remaining $\approx 70\%$ (Fig. 7). The cause of this decrease in NEP was split evenly between a decrease in NPP and an increase in HR. The higher NPP in the counterfactual compared to the original DS_{CCI} simulation was associated with 13 PgC more vegetation carbon in 2008, while the reduction in HR was associated with a slightly increased soil carbon pool of 1 PgC.

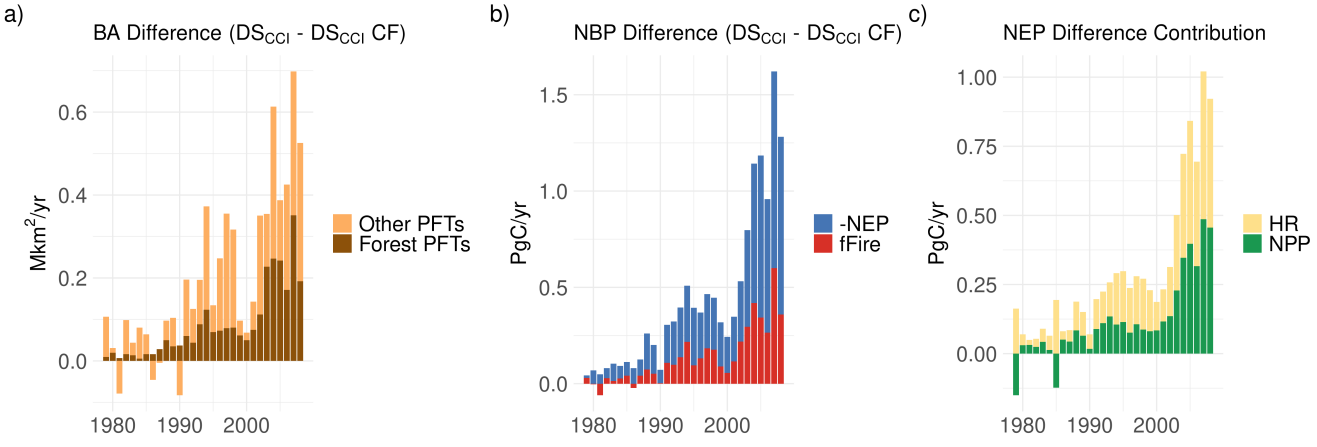

Figure 7. Differences between JULES global BA, NBP and NEP estimates globally between the standard DS_{CCI} and counterfactual (DS_{CCI} CF) across 1979–2008. BA differences are split between forest and non-forest PFTs (panel a), while differences in NBP are split between NEP and fire emissions (panel b) and NEP differences are split between NPP and HR (panel c).

The magnitude of year-to-year differences in NBP between the counterfactual and original simulations were aligned much more closely with year to year differences in forest BA rather than total BA (Fig. 7). Furthermore, differences in burned area in forest PFTs accounted for a large proportion of the spatial variability in NBP difference between the original and counterfactual simulations on average over 1978–2008 ($R^2 = 0.83$), while differences in total burned area accounted for a much lower proportion ($R^2 = 0.25$). This suggests that forest BA dynamics in particular have a high impact on JULES NBP estimates.

https://doi.org/10.5194/egusphere-2026-3584
Preprint. Discussion started: 30 June 2026
© Author(s) 2026. CC BY 4.0 License.

The increase in burned area caused a reduction of 0.9 PgC year^{-1} over 2000–2008. Therefore, the counterfactual NBP was 2.7 PgC year^{-1} over this period which is similar to the PS average of 2.6 PgC year^{-1} and lies well within 1 S.D of the mean of the GCB inversions and close to the GCB residual sink.

5 Discussion

5.1 Multi-model

5.1.1 Fire emission estimates

When applying long-term diagnostic burned area across the five DGVMs, we found large spatial and regional improvements were made to fire emission estimates against observation-based estimates, while retaining realistic land sink estimates and smooth burned area transitions. Although global burned area and fire emission estimates were similar on average under diagnostic burned area, the reduction in spatial and regional biases were substantial. For example, the fire emission biases under prognostic BA of underestimation in African savannas, and overestimation across much of Eurasia (also seen in FireMIP analyses, Hantson et al., 2016) were substantially reduced under diagnostic BA. These improvements could be especially relevant to regional carbon budgets, where regional fire disturbance and fire emission biases may have significant impacts on DGVM carbon cycle estimates. Additionally, the inter-model spread in global fire emissions is reduced by more than a factor of 2 under diagnostic burned area compared to prognostic, meaning by implementing diagnostic burned area in DGVMs, we can significantly reduce the inter-model uncertainty around the short term impacts of fire on the carbon cycle.

Contrastingly, when implementing diagnostic burned areas in DGVMs we failed to reduce the inter-model spread around global fire combustion rate estimates (fire emissions per unit BA), despite spatially consistent burned areas. Furthermore, inter-model spread remained high regionally, and in many regions spread increased under diagnostic BA. This increased spread is probably attributable to compensation effects due to coupling between BA, fuel loads and fire emissions in prognostic BA simulations. Under diagnostic BA, this coupling is removed, allowing model differences in fuel availability and combustion processes to fully manifest. Also, in many regions magnitudes and trends aligned poorly compared to the GFED "natural" products. This highlights the high level of variability in simulated fuel loads, combustion completeness, and post-fire impacts such as fire-induced tree mortality in models (Table 2).

For example, in moist tropical regions, such as South and Central America and Equatorial Asia, inter-model spread is large, and fire combustion rates are high compared to GFED estimates on average. This implies that simulated available fuel loads or combustion completeness are also highly variable and possibly overestimated by the DGVMs on average in these regions. This aligns well with the work of Forkel et al., 2025, which concludes that the majority of fire emissions in the Amazon and Cerrado are from the smoldering of woody debris, with litter burning making up a smaller proportion, and the burning of herbaceous material forming a near negligible proportion of total CO_2 emissions. On the other hand, all participating models except ORCHIDEE base fuel loads either directly or indirectly on vegetation biomass. Therefore, the DGVMs in our analysis may be misrepresenting fuel contents in moist tropical regions, with potentially too high a proportion of live vegetation biomass. For

https://doi.org/10.5194/egusphere-2026-3584
Preprint. Discussion started: 30 June 2026
© Author(s) 2026. CC BY 4.0 License.

example, in the JULES model around 1 third of fire emissions in SHSA under diagnostic burned area came from vegetation combustion. Furthermore, an explicit woody debris pool is not simulated by JULES meaning it has a fundamental problem when estimating fire emissions and carbon pool impacts in these regions.

Alternatively, combustion completeness values and dependencies vary across the DGVMs used in our analysis, with two of the five models varying combustion completeness (CC) with soil or fuel moisture (JULES, ORCHIDEE), and three using fixed values per PFT, biome or biomass pool (EDv3, VISIT-UT, OCN) (Table 2). These differences in CC may increase variability in simulated fire combustion rates, with differences in the handling of fuel moisture possibly having a large impact in moist tropical ecosystems where fuels are often subjected to seasonal drying and droughts (Aragão et al., 2018).

On the other hand, in boreal regions, the fire combustion rate is underestimated by more than a factor of 2 compared to GFED estimates, values stated in Zheng et al., 2021 and Jones et al., 2024, and field measurements (van Leeuwen et al., 2014; van Wees et al., 2022). In these regions, forest fires are generally severe stand replacing events, characterised by high intensity crown fires which cause high levels of fire-induced mortality and combustion completeness (Amiro et al., 2006; Xu et al., 2024; Webb et al., 2024). These fires may also burn deep into the duff layer and soils, leading to the combustion of soil organic carbon (SOC), which can contribute to a large proportion of total fire emissions (Walker et al., 2018; Boby et al., 2010). In four of the five participating models (JULES, EDv3, VISIT-UT, OCN), fire intensity is not calculated and fire-induced mortality is kept as a constant proportion across all forest PFTs and biomes. Fire emissions are then calculated based on fuel loads and vegetation burned by fire, scaled with combustion completeness (Table 2). In EDv3, mortality does vary based on tree height (an observed relationship, Balch et al., 2011), but this does not differ based on forest type or location. In ORCHIDEE, fire intensity (fireline intensity, kWm^{-1}, estimated based on fire rate of spread and fuel loads) is used to estimate scorch height, from which the level of fire-induced mortality through crown damage and cambium death is calculated. However, vegetation killed by fire does not form a component of fire emissions in ORCHIDEE, so variations in fire-induced mortality do not impact fire emission estimates. Also, in all our participating models below-surface soil organic carbon is unavailable to fires, meaning this significant component of the fuel load in boreal forests is unaccounted for in these models. This potential underestimation of fire-induced mortality combined with a lack of SOC combustion means that fire combustion rates (and fire emissions) are probably underestimated by models in boreal regions, where fire intensity and severity is generally high and below-surface SOC may become available to fire.

In addition, GFED estimates, along with other bottom-up estimates (Jones et al., 2024), and top-down estimates (Zheng et al., 2021), show an increasing global trend in fire combustion rates, attributed to an increase in forest fire intensity and burned area. Specifically, this increase is linked to climate change induced changes to forest fire regimes in the extratropics (Jones et al., 2024; Fan et al., 2022), partly associated with increases in extreme fire events (Cunningham et al., 2024). Under diagnostic burned area, our models failed to replicate the magnitude of this positive trend, especially in Boreal Asia. Although uncertainties exist around the partitioning of burned area across different land cover classes in both our methodology and burned area products (Chuvieco et al., 2019; Lizundia-Loiola et al., 2020), in fire-prone boreal regions woody land cover dominates (Flannigan et al., 2009; Helbig et al., 2024), suggesting the partitioning of burned area across different land cover classes is less uncertain in these regions. Also, in the GFED5 product (where burned area land cover partitions are provided),

https://doi.org/10.5194/egusphere-2026-3584
Preprint. Discussion started: 30 June 2026
© Author(s) 2026. CC BY 4.0 License.

no significant trend in boreal forest burned area is observed in Boreal Asia, while a significant positive trend in boreal forest fire combustion rate is present. This implies that changes to fire intensity and combustion completeness, rather than burned area partitioning, are probably driving this increase in fire combustion rate in Boreal Asia. This further emphasizes the need for models to produce estimates of fire intensity and relate these to emissions in order to better replicate observed magnitudes and trends in fire combustion rates.

On the other hand, in Australia, DGVMs were able to capture the spike in fire combustion rate and fire emissions in 2019 and 2020 associated with the "Black Summer" extreme fire event (Ahmed and Ledger, 2023; Udy et al., 2024). This highlights the ability of DGVM models to capture certain extreme fire events when diagnostic BA is used, providing insight into the overall impact of these events on the carbon cycle. This may be particularly useful to regional carbon budgets, where extreme fire events may have a significant impact on the carbon cycle over long time periods.

5.1.2 Land sink estimates

The reduction to the DGVM global land sink estimate observed under diagnostic BA over 2001–2020 led to closer agreement with the GCB inversions (corrected for land-use emissions and the river flux) and residual sink on average, however this result was not shared across models and inter-model spread remained high. Around half of this reduction stemmed from Africa, bringing land sink estimates more in line with inversions. This may be due to better constrained biomass in African savanna regions on average under diagnostic BA (Fig. S4), associated with a higher level of fire disturbance.

Under diagnostic BA, the significant positive trend present in the land sink over 2001–2020 in three of the models was mainly attributable to negative trends in fire emissions, as well as a positive trend in NEP in the JULES model (associated with the decrease in global burned area over the start of the 21st century). If models were able to capture the observed positive trend in fire combustion rate, fire emission estimates would decrease at a lower rate in the diagnostic BA simulations, meaning we would expect these positive land sink trends to be of a lower magnitude and more in line with top-down constraints and the GCB residual sink.

5.1.3 JULES sensitivity experiment

When diagnosing BA in the JULES DGVM with both the GFED5 and FireCCI5.1 based reconstructions, we found the choice of diagnostic BA led to a substantial difference in modern day land sink estimates (0.8 PgC year^{-1} on average over 2001–2020). This result differs from Poulter et al., 2015, which found land sink estimates from the LPJ model remained stable when three distinct satellite BA products were applied, however in this study differences in long-term BA dynamics were not present.

Fire emission estimates also differed significantly between the simulations (1.1 PgC year^{-1}), and scaled well depending on the choice of reconstruction (close agreement between DS_{GFED} and GFED5, and between DS_{CCI} and GFED4.1s). However, these differences in fire emissions between simulations are not directly responsible for the differences in NBP, since the model was spun-up to a different "pre-industrial" equilibrium, with NBP equal to zero in both simulations.

Based on visual assessment and the counterfactual simulation, described in Table 1, we suggest that the differences in modern day NBP between the simulations are mainly attributable to differences in 20th century burned area dynamics (especially in

https://doi.org/10.5194/egusphere-2026-3584
Preprint. Discussion started: 30 June 2026
© Author(s) 2026. CC BY 4.0 License.

forest PFTs) having a legacy effect on land sink estimates. Specifically, the counterfactual showed that the increase in burned area between 1979 and 2008 present in the FireCCI5.1 reconstruction led to a substantially reduced land sink estimate over the 2000–2008 period in the FireCCI5.1 diagnostic BA simulation (-0.9 PgC year^{-1}). This suggests that without this increase in burned area the FireCCI5.1 diagnostic BA simulation modern day land sink estimate would be similar to the prognostic simulation average, and align well with the GCB inversions and GCB residual. In the GFED5 diagnostic BA simulation, the rise in burned area over 1979–2003 is of greater magnitude than that of the FireCCI5.1 reconstruction, and burned area does not decrease over 1901–1978 (Fig. 6a). These differences in past BA dynamics between the reconstructions are the most plausible explanation for the lower modern day land sink magnitude in this simulation.

The majority of the NBP difference between the counterfactual and standard FireCCI5.1 diagnostic BA simulations in JULES stemmed from changes to NEP, rather than just differences in fire emissions. This finding is similar to that in Yin et al., 2020, which predicts that the observed drop in global burned area between 2008–2014 compared to 2001–2007 leads to an increase in the land sink of 0.6 PgC year^{-1} across 2008–2014, with just 0.2 PgC year^{-1} of this change resulting from fire emission changes and the remaining 0.4 PgC year^{-1} resulting from changes to NEP (based on model land sink estimates from the CARDAMOM DGVM). This effect on NEP is due to decreased fire disturbances leading to a reduction in heterotrophic respiration (due to a reduction in litter/soil pool inputs through fire-induced mortality), as well as an increase in NPP (due to increases in biomass and photosynthetic capacity). Our analysis suggests that BA dynamics in forest ecosystems specifically are probably the main driver of changes to NBP. This may be expected since simulated fuel loads are generally high in forest ecosystems. Also, photosynthetic capacity is high in forests, and a large amount of carbon is lost to litter/soil pools when fire-induced mortality occurs due to the high biomass. Hence, BA dynamics in forest ecosystems may be expected to have an especially large impact on NEP.

Overall, this implies that pre-satellite era burned area dynamics may have a significant impact on modern day land sink estimates in DGVMs, with an average disparity in JULES NBP estimates of 0.8 PgC year^{-1} over 2001–2020 depending which of the two burned area reconstructions is used. However, this impact may be substantially lower in other models depending how fire dynamics impact ecosystem productivity, highlighting the need for further investigation into the true impact of fire regime changes on NEP.

5.2 Implications for future work and the Global Carbon Budget

In the context of GCB and the TRENDY project, our results imply diagnostic burned area simulations may offer advantages over the current default of simulations with prognostic BA. Improved burned area realism across models led to a lower inter-model uncertainty around fire emission estimates, along with significant reductions in many regional fire emission biases, and moderate improvements to net land sink estimates compared to prognostic BA simulations. Also, the improved ability to capture extreme fire events and their impact on the carbon cycle may be especially valuable, given the increasing frequency and severity of these events and their potentially significant impacts on regional carbon cycling (Cunningham et al., 2024; Walker et al., 2018). However, our sensitivity experiment in JULES showed that underlying uncertainties in burned area mapping and pre-satellite era burned area dynamics may add a high level of uncertainty to net land sink estimates, which may be overlooked when

https://doi.org/10.5194/egusphere-2026-3584
Preprint. Discussion started: 30 June 2026
© Author(s) 2026. CC BY 4.0 License.

uniform burned area is diagnosed across models. Specifically, the unrealistically low JULES NBP estimate under the GFED5 reconstruction, probably driven by pre-satellite burned area dynamics, suggests that the land sink improvements observed under diagnostic BA may not be robust to differing burned area reconstructions and mappings. In addition, practical obstacles must be overcome in order for diagnostic burned area to be adopted as the default in GCB and TRENDY. For example, currently only a small subset of DGVMs involved in the TRENDY project are capable of performing diagnostic BA simulations, so further development is needed to implement diagnostic BA across all models. Furthermore, few satellite burned area products have a sufficiently low latency to cover the previous year in full, which is a crucial year for GCB analyses.

In the multi-model analysis, we showed that even under diagnostic BA models generally fail to capture the documented global positive trend in fire combustion rate, meaning carbon budget estimates produced using DGVMs with diagnostic burned area may not account for observed increases in fire intensity and forest fire occurrence. Regionally, fire combustion rate magnitudes were also poorly replicated and highly variable. This exposes the need for models to better estimate available fuel loads and fuel composition, combustion completeness, and post-fire impacts such as fire-induced mortality, and to vary these impacts based on regional fire regimes. In order to better constrain modelled fire combustion rates, the DGVM community could look toward field measurements of fuel consumption, such as the database of van Leeuwen et al., 2014 (updated by van Wees et al., 2022). Also, the lack of positive trend in fire combustion rates in boreal regions (particularly in Boreal Asia, present in GFED estimates and documented by Jones et al., 2024, Zheng et al., 2021) highlights the need for DGVMs to estimate forest fire intensity and relate this to fire emissions, in order to produce realistic fire emission changes with the changing climate. Fire intensity has also been shown to correlate with other factors affecting the impact of a fire on ecosystems and the carbon cycle, such as the level of fire-induced mortality (Balch et al., 2011), further demanding its inclusion in DGVM fire modules. In addition, the fire combustion rate underestimation in boreal regions may arise in part from insufficient burning of soil organic carbon, indicating that models need to make soil organic carbon available to fire in order to represent fire carbon cycle impacts effectively in these regions.

Our JULES sensitivity experiment results motivate further work into the impact of long-term fire dynamics on contemporary NBP. Realistic and accurate historical burned area datasets are needed. Further, more research is needed into the cascading impacts of fires, from direct emissions, to delayed mortality and shifts in plant community composition.

In JULES a large proportion of the biomass killed by fire enters the soil pools, specifically the fast decaying decomposable and resistant plant matter pools (DPM and RPM). This can lead to a large and sudden increase in heterotrophic respiration post-fire, especially in forest PFTs where the amount of biomass killed by fire is high. On the other hand, the decay time of large woody biomass killed by fire occurs over long timescales (with 85% of killed biomass carbon observed to be persisting 10 years after a large Oregon wildfire, Campbell et al., 2016). Furthermore, a significant proportion of burned biomass is converted to inert pyrogenic carbon post-fire (around 28% of charred carbon after a typical boreal forest fire, Santín et al., 2014), leading to an increased soil carbon sink on millennial timescales (Bowring et al., 2022). This process is currently unaccounted for in JULES. All this suggests that increases in heterotrophic respiration post-fire disturbance in JULES may be too high. Therefore, the effect of changes to fire regime on NEP may be overestimated in the JULES DGVM, but more research is needed to prove

https://doi.org/10.5194/egusphere-2026-3584
Preprint. Discussion started: 30 June 2026
© Author(s) 2026. CC BY 4.0 License.

this (especially as changes to NPP post-fire are also highly uncertain). In addition, 20th century BA dynamics between the two reconstructions differ markedly (Fig. 1), adding to the uncertainty around DGVM land sink estimates under diagnostic BA.

6 Conclusions

In conclusion, by applying long-term diagnostic burned area to a subset of five DGVMs in TRENDY, this study shows that fire emission estimate realism and constraint across models can be substantially improved when diagnostic burned area is applied rather than prognostic (59% reduction in inter-model S.D and large reductions to regional biases observed), in turn reducing inter-model uncertainty around the immediate impacts of fires on the carbon cycle. Contrastingly, we found that land sink estimate realism may be moderately improved under diagnostic BA, but inter-model uncertainty may remain similar between diagnostic and prognostic burned area simulations despite fire emission improvements.

Furthermore, this study demonstrates that fire-enabled DGVMs are currently unable to capture the changing nature of fire regimes and impacts on carbon dioxide emissions even under diagnostic burned areas, impacting land sink estimates and dynamics. This arises from the poor representation of fuel loads and fuel composition, combustion completeness, fire-induced tree mortality, and the influence of fire intensity on fire emissions. Specifically, in forested regions ecosystem-level differences in fire regime and post-fire impacts are poorly represented, affecting regional carbon budget accuracy. Additionally, the fact that the observed global increase in fire combustion rate is not captured influences global land sink trends, highlighting the need to reproduce these trends effectively in models.

Also, by applying two long-term diagnostic burned area reconstructions to the JULES DGVM, this study demonstrates that DGVM fire emission estimates scale realistically depending on the burned area product used. However, land sink estimates varied substantially between the diagnostic burned area simulations (differing by 0.8 PgC year^{-1} on average over 2001–2020), probably due to differences in burned area dynamics across the 20th century between the two reconstructions having legacy effects on both fire emission and NEP estimates (evidenced by the use of a counterfactual simulation). This indicates that a potentially high level of uncertainty around modern day land sink estimates in DGVMs is attributable to pre-satellite era burned area dynamics, highlighting the need for further investigation into the effects that burned area dynamics have on the carbon cycle and the uncertainty around past burned area trends.

7 Data availability

GFED5 and GFED4.1s data used in this study are publicly available from https://www.globalfiredata.org/data.html (last access: 9 June 2026) (Werf et al., 2025; van der Werf et al., 2017), and GCB inversion and land-use change datasets are available from https://www.icos-cp.eu/data-products/global-co2-gridded-flux-fields-14-atmospheric-inversions-gcb2025, https://globalcarbonbudget.org/the-latest-gcb-data/ (last access: 9 June 2026) (Luijkx et al., 2024; Friedlingstein et al., 2025b). Reconstructed burned area datasets are available from https://zenodo.org/records/14191467 (last access: 9 June 2026) (Guo et al.,

https://doi.org/10.5194/egusphere-2026-3584
Preprint. Discussion started: 30 June 2026
© Author(s) 2026. CC BY 4.0 License.

2025). TRENDY model simulations are hosted by Michael O'Sullivan and are available from https://mdosullivan.github.io/GCB/ (last access: 9 June 2026) (Sitch et al., 2024; Friedlingstein et al., 2025b).

8 Author contribution

W.L., S.S., P.F. and P.C. conceived the original idea. W.L., Z.G., S.S., P.F., M.O. and T.S. contributed to study design and methodology. A.B., J.G.d.S., Z.G., A.I., W.L., L.M., M.O. and T.S. were involved in performing the model simulations used in the analyses. T.S. carried out the formal analyses and wrote the first draft. S.S, P.F. and M.O. supervised the work. All authors reviewed the manuscript and contributed to its final form.

9 Competing interests

The contact author has declared that none of the authors has any competing interests.

10 Acknowledgements

This work was funded by Schmidt Sciences as part of the VESRI CALIPSO and VICC CLARiTy projects (USA). Further support was received from the THRAC3E project (grant no. 4000149569/25/I-AG) (European Space Agency), RECCAP2-CS (grant no. 4000144908/24/1-LR) (European Space Agency), the XFires project (contract no. 4000145351/24/I-LR) (European Space Agency), and the Amazon-SOS project (grant no. NE/X019055/1) (NERC). AB acknowledges funding from the European Research Council (ERC StG, ForExD, grant agreement No. 101039567). For the purpose of open access, the author has applied a Creative Commons Attribution (CC BY) license to any Author Accepted Manuscript version arising from this submission.

https://doi.org/10.5194/egusphere-2026-3584
Preprint. Discussion started: 30 June 2026
© Author(s) 2026. CC BY 4.0 License.

References

Ahmed, I. and Ledger, K.: Lessons from the 2019/2020 'Black Summer Bushfires' in Australia, International Journal of Disaster Risk Reduction, 96, 103 947, https://doi.org/10.1016/j.ijdrr.2023.103947, 2023.

Akagi, S. K., Yokelson, R. J., Wiedinmyer, C., Alvarado, M. J., Reid, J. S., Karl, T., Crounse, J. D., and Wennberg, P. O.: Emission factors for open and domestic biomass burning for use in atmospheric models, Atmospheric Chemistry and Physics, 11, 4039–4072, https://doi.org/10.5194/acp-11-4039-2011, 2011.

Amiro, B., Orchansky, A., Barr, A., Black, T., Chambers, S., Chapin III, F., Goulden, M., Litvak, M., Liu, H., McCaughey, J., McMillan, A., and Randerson, J.: The effect of post-fire stand age on the boreal forest energy balance, Agricultural and Forest Meteorology, 140, 41–50, https://doi.org/10.1016/j.agrformet.2006.02.014, the Fluxnet-Canada Research Network: Influence of Climate and Disturbance on Carbon Cycling in Forests and Peatlands, 2006.

Andela, N., Morton, D. C., Giglio, L., Chen, Y., van der Werf, G. R., Kasibhatla, P. S., DeFries, R. S., Collatz, G. J., Hantson, S., Kloster, S., Bachelet, D., Forrest, M., Lasslop, G., Li, F., Mangeon, S., Melton, J. R., Yue, C., and Randerson, J. T.: A human-driven decline in global burned area, Science, 356, 1356–1362, https://doi.org/10.1126/science.aal4108, 2017.

Aragão, L., Anderson, L., Fonseca, M., Rosan, T. M., Vedovato, L., Wagner, F., Silva, C., Silva-Junior, C., Arai, E., Aguiar, A. P., Barlow, J., Berenguer, E., Deeter, M., Domingues, L., Gatti, L., Gloor, M., Malhi, Y., Marengo, J., Miller, J., and Saatchi, S.: 21st Century drought-related fires counteract the decline of Amazon deforestation carbon emissions, Nature Communications, 9, 536, https://doi.org/10.1038/s41467-017-02771-y, 2018.

Archibald, S., Lehmann, C. E. R., Belcher, C. M., Bond, W. J., Bradstock, R. A., Daniau, A.-L., Dexter, K. G., Forrestel, E. J., Greve, M., He, T., Higgins, S. I., Hoffmann, W. A., Lamont, B. B., McGlinn, D. J., Moncrieff, G. R., Osborne, C. P., Pausas, J. G., Price, O., Ripley, B. S., Rogers, B. M., Schwilk, D. W., Simon, M. F., Turetsky, M. R., Van der Werf, G. R., and Zanne, A. E.: Biological and geophysical feedbacks with fire in the Earth system, Environmental Research Letters, 13, 033 003, https://doi.org/10.1088/1748-9326/aa9ead, 2018.

Balch, J. K., Nepstad, D. C., Curran, L. M., Brando, P. M., Portela, O., Guilherme, P., Reuning-Scherer, J. D., and de Carvalho, O.: Size, species, and fire behavior predict tree and liana mortality from experimental burns in the Brazilian Amazon, Forest Ecology and Management, 261, 68–77, https://doi.org/10.1016/j.foreco.2010.09.029, 2011.

Best, M. J., Pryor, M., Clark, D. B., Rooney, G. G., Essery, R. L. H., Ménard, C. B., Edwards, J. M., Hendry, M. A., Porson, A., Gedney, N., Mercado, L. M., Sitch, S., Blyth, E., Boucher, O., Cox, P. M., Grimmond, C. S. B., and Harding, R. J.: The Joint UK Land Environment Simulator (JULES), model description – Part 1: Energy and water fluxes, Geoscientific Model Development, 4, 677–699, https://doi.org/10.5194/gmd-4-677-2011, 2011.

Boby, L. A., Schuur, E. A. G., Mack, M. C., Verbyla, D., and Johnstone, J. F.: Quantifying fire severity, carbon, and nitrogen emissions in Alaska's boreal forest, Ecological Applications, 20, 1633–1647, https://doi.org/10.1890/08-2295.1, 2010.

Bond, W. J., Woodward, F. I., and Midgley, G. F.: The global distribution of ecosystems in a world without fire, New Phytologist, 165, 525–538, https://doi.org/10.1111/j.1469-8137.2004.01252.x, 2005.

Bowman, D. M. J. S., Balch, J. K., Artaxo, P., Bond, W. J., Carlson, J. M., Cochrane, M. A., D'Antonio, C. M., DeFries, R. S., Doyle, J. C., Harrison, S. P., Johnston, F. H., Keeley, J. E., Krawchuk, M. A., Kull, C. A., Marston, J. B., Moritz, M. A., Prentice, I. C., Roos, C. I., Scott, A. C., Swetnam, T. W., van der Werf, G. R., and Pyne, S. J.: Fire in the Earth System, Science, 324, 481–484, https://doi.org/10.1126/science.1163886, 2009.

https://doi.org/10.5194/egusphere-2026-3584
Preprint. Discussion started: 30 June 2026
© Author(s) 2026. CC BY 4.0 License.

Bowring, S., Jones, M., Ciais, P., Guenet, B., and Abiven, S.: Pyrogenic carbon decomposition critical to resolving fire's role in the Earth system, Nature Geoscience, 15, 135–142, https://doi.org/10.1038/s41561-021-00892-0, 2022.

Burton, C., Betts, R., Cardoso, M., Feldpausch, T. R., Harper, A., Jones, C. D., Kelley, D. I., Robertson, E., and Wiltshire, A.: Representation of fire, land-use change and vegetation dynamics in the Joint UK Land Environment Simulator vn4.9 (JULES), Geoscientific Model Development, 12, 179–193, https://doi.org/10.5194/gmd-12-179-2019, 2019.

Burton, C., Kelley, D., Burke, E., Mathison, C., Jones, C., Betts, R., Robertson, E., Teixeira, J., Cardoso, M., and Anderson, L.: Fire weakens land carbon sinks before 1.5 °C, Nature Geoscience, 17, 1108–1114, https://doi.org/10.1038/s41561-024-01554-7, 2024.

Campbell, J. L., Fontaine, J. B., and Donato, D. C.: Carbon emissions from decomposition of fire-killed trees following a large wildfire in Oregon, United States, Journal of Geophysical Research: Biogeosciences, 121, 718–730, https://doi.org/10.1002/2015JG003165, 2016.

Chen, Y., Hall, J., Van Wees, D., Andela, N., Hantson, S., Giglio, L., Van Der Werf, G. R., Morton, D. C., and Randerson, J. T.: Multi-decadal trends and variability in burned area from the 5th version of the Global Fire Emissions Database (GFED5), Earth System Science Data Discussions, 2023, 1–52, 2023.

Chuvieco, E., Mouillot, F., van der Werf, G. R., San Miguel, J., Tanase, M., Koutsias, N., García, M., Yebra, M., Padilla, M., Gitas, I., Heil, A., Hawbaker, T. J., and Giglio, L.: Historical background and current developments for mapping burned area from satellite Earth observation, Remote Sensing of Environment, 225, 45–64, https://doi.org/10.1016/j.rse.2019.02.013, 2019.

Clark, D. B., Mercado, L. M., Sitch, S., Jones, C. D., Gedney, N., Best, M. J., Pryor, M., Rooney, G. G., Essery, R. L. H., Blyth, E., Boucher, O., Harding, R. J., Huntingford, C., and Cox, P. M.: The Joint UK Land Environment Simulator (JULES), model description – Part 2: Carbon fluxes and vegetation dynamics, Geoscientific Model Development, 4, 701–722, https://doi.org/10.5194/gmd-4-701-2011, 2011.

Cunningham, C., Williamson, G., and Bowman, D.: Increasing frequency and intensity of the most extreme wildfires on Earth, Nature Ecology Evolution, 8, 1420–1425, https://doi.org/10.1038/s41559-024-02452-2, 2024.

Ermitão, T., Gouveia, C., Russo, A., Burton, C., Churiulin, E., Souza, J., O'Sullivan, M., Ciais, P., Zaehle, S., Sitch, S., Li, W., Xu, Y., and Bastos, A.: Influence of simulated vs. satellite-based burned areas on modelled terrestrial carbon fluxes, Carbon Balance and Management, 21, https://doi.org/10.1186/s13021-025-00366-5, 2026.

ESA: Land Cover CCI Product User Guide Version 2, Tech. rep., http://maps.elie.ucl.ac.be/CCI/viewer/download/ESACCI-LC-Ph2-PUGv2_2.0.pdf, 2017.

Fan, L., Wigneron, J.-P., Ciais, P., Chave, J., Brandt, M., Sitch, S., Yue, C., Bastos, A., Li, X., Qin, Y., Yuan, W., Schepaschenko, D., Mukhortova, L., Li, X., Liu, X., Mengjia, W., Frappart, F., Xiao, X., Chen, J., and Fensholt, R.: Siberian carbon sink reduced by forest disturbances, Nature Geoscience, 16, 1–7, https://doi.org/10.1038/s41561-022-01087-x, 2022.

Flannigan, M., Stocks, B., Turetsky, M., and Wotton, M.: Impacts of climate change on fire activity and fire management in the circumboreal forest, Global Change Biology, 15, 549–560, https://doi.org/10.1111/j.1365-2486.2008.01660.x, 2009.

Forkel, M., Wessollek, C., Huijnen, V., Andela, N., Laat, A., Kinalczyk, D., Marrs, C., van Wees, D., Bastos, A., Ciais, P., Fawcett, D., Kaiser, J., Klauberg, C., Kutchartt, E., Leite, R., Li, W., Sitch, S., Souza, J., and Plummer, S.: Burning of woody debris dominates fire emissions in the Amazon and Cerrado, Nature Geoscience, 18, 140–147, https://doi.org/10.1038/s41561-024-01637-5, 2025.

Friedlingstein, P., O'Sullivan, M., Jones, M. W., Andrew, R. M., Bakker, D. C. E., Hauck, J., Landschützer, P., Le Quéré, C., Li, H., Luijkx, I. T., Peters, G. P., Peters, W., Pongratz, J., Schwingshackl, C., Sitch, S., Canadell, J. G., Ciais, P., Aas, K., Alin, S. R., Anthoni, P., Barbero, L., Bates, N. R., Bellouin, N., Benoit-Cattin, A., Berghoff, C. F., Bernardello, R., Bopp, L., Brasika, I. B. M., Chamberlain, M. A., Chandra, N., Chevallier, F., Chini, L. P., Collier, N. O., Colligan, T. H., Cronin, M., Djeutchouang, L., Dou, X., Enright, M. P., Enyo, K., Erb, M., Evans, W., Feely, R. A., Feng, L., Ford, D. J., Foster, A., Fransner, F., Gasser, T., Gehlen, M., Gkritzalis, T., Goncalves

https://doi.org/10.5194/egusphere-2026-3584
Preprint. Discussion started: 30 June 2026
© Author(s) 2026. CC BY 4.0 License.

De Souza, J., Grassi, G., Gregor, L., Gruber, N., Guenet, B., Gürses, O., Harrington, K., Harris, I., Heinke, J., Hurtt, G. C., Iida, Y., Ilyina, T., Ito, A., Jacobson, A. R., Jain, A. K., Jarníková, T., Jersild, A., Jiang, F., Jones, S. D., Kato, E., Keeling, R. F., Klein Goldewijk, K., Knauer, J., Kong, Y., Korsbakken, J. I., Koven, C., Kunimitsu, T., Lan, X., Liu, J., Liu, Z., Liu, Z., Lo Monaco, C., Ma, L., Marland, G., McGuire, P. C., McKinley, G. A., Melton, J., Monacci, N., Monier, E., Morgan, E. J., Munro, D. R., Müller, J. D., Nakaoka, S.-I., Nayagam, L. R., Niwa, Y., Nutzel, T., Olsen, A., Omar, A. M., Pan, N., Pandey, S., Pierrot, D., Qin, Z., Regnier, P. A. G., Rehder, G., Resplandy, L., Roobaert, A., Rosan, T. M., Rödenbeck, C., Schwinger, J., Skjelvan, I., Smallman, T. L., Spada, V., Sreeush, M. G., Sun, Q., Sutton, A. J., Sweeney, C., Swingedouw, D., Séférian, R., Takao, S., Tatebe, H., Tian, H., Tian, X., Tilbrook, B., Tsujino, H., Tubiello, F., van Ooijen, E., van der Werf, G., van de Velde, S. J., Walker, A., Wanninkhof, R., Yang, X., Yuan, W., Yue, X., and Zeng, J.: Global Carbon Budget 2025, Earth System Science Data Discussions, 2025, 1–139, https://doi.org/10.5194/essd-2025-659, 2025a.

Friedlingstein, P., O'Sullivan, M., Jones, M. W., Andrew, R. M., Hauck, J., Landschützer, P., Le Quéré, C., Li, H., Luijkx, I. T., Olsen, A., Peters, G. P., Peters, W., Pongratz, J., Schwingshackl, C., Sitch, S., Canadell, J. G., Ciais, P., Jackson, R. B., Alin, S. R., Arneth, A., Arora, V., Bates, N. R., Becker, M., Bellouin, N., Berghoff, C. F., Bittig, H. C., Bopp, L., Cadule, P., Campbell, K., Chamberlain, M. A., Chandra, N., Chevallier, F., Chini, L. P., Colligan, T., Decayeux, J., Djeutchouang, L. M., Dou, X., Duran Rojas, C., Enyo, K., Evans, W., Fay, A. R., Feely, R. A., Ford, D. J., Foster, A., Gasser, T., Gehlen, M., Gkritzalis, T., Grassi, G., Gregor, L., Gruber, N., Gürses, O., Harris, I., Hefner, M., Heinke, J., Hurtt, G. C., Iida, Y., Ilyina, T., Jacobson, A. R., Jain, A. K., Jarníková, T., Jersild, A., Jiang, F., Jin, Z., Kato, E., Keeling, R. F., Klein Goldewijk, K., Knauer, J., Korsbakken, J. I., Lan, X., Lauvset, S. K., Lefèvre, N., Liu, Z., Liu, J., Ma, L., Maksyutov, S., Marland, G., Mayot, N., McGuire, P. C., Metzl, N., Monacci, N. M., Morgan, E. J., Nakaoka, S.-I., Neill, C., Niwa, Y., Nützel, T., Olivier, L., Ono, T., Palmer, P. I., Pierrot, D., Qin, Z., Resplandy, L., Roobaert, A., Rosan, T. M., Rödenbeck, C., Schwinger, J., Smallman, T. L., Smith, S. M., Sospedra-Alfonso, R., Steinhoff, T., Sun, Q., Sutton, A. J., Séférian, R., Takao, S., Tatebe, H., Tian, H., Tilbrook, B., Torres, O., Tourigny, E., Tsujino, H., Tubiello, F., van der Werf, G., Wanninkhof, R., Wang, X., Yang, D., Yang, X., Yu, Z., Yuan, W., Yue, X., Zaehle, S., Zeng, N., and Zeng, J.: Global Carbon Budget 2024, Earth System Science Data, 17, 965–1039, https://doi.org/10.5194/essd-17-965-2025, 2025b.

Gasser, T., Crepin, L., Quilcaille, Y., Houghton, R. A., Ciais, P., and Obersteiner, M.: Historical CO_2 emissions from land use and land cover change and their uncertainty, Biogeosciences, 17, 4075–4101, https://doi.org/10.5194/bg-17-4075-2020, 2020.

Giglio, L., Schroeder, W., and Justice, C. O.: The collection 6 MODIS active fire detection algorithm and fire products, Remote Sensing of Environment, 178, 31–41, https://doi.org/10.1016/j.rse.2016.02.054, 2016.

Gomes, L., Sinátora, H., Filho, B., Rodrigues, L., Oliveira, U., and Bustamante, M.: Responses of Plant Biomass in the Brazilian Savanna to Frequent Fires, Frontiers in Forests and Global Change, 3, https://doi.org/10.3389/ffgc.2020.507710, 2020.

Guimberteau, M., Zhu, D., Maignan, F., Huang, Y., Yue, C., Dantec-Nédélec, S., Ottlé, C., Jornet-Puig, A., Bastos, A., Laurent, P., Goll, D., Bowring, S., Chang, J., Guenet, B., Tifafi, M., Peng, S., Krinner, G., Ducharne, A., Wang, F., Wang, T., Wang, X., Wang, Y., Yin, Z., Lauerwald, R., Joetzjer, E., Qiu, C., Kim, H., and Ciais, P.: ORCHIDEE-MICT (v8.4.1), a land surface model for the high latitudes: model description and validation, Geoscientific Model Development, 11, 121–163, https://doi.org/10.5194/gmd-11-121-2018, 2018.

Guo, Z., Li, W., Ciais, P., Sitch, S., van der Werf, G. R., Bowring, S. P. K., Bastos, A., Mouillot, F., He, J., Sun, M., Zhu, L., Du, X., Wang, N., and Huang, X.: Reconstructed global monthly burned area maps from 1901 to 2020, Earth System Science Data Discussions, 2025, 1–28, https://doi.org/10.5194/essd-2024-556, 2025.

Hansis, E., Davis, S. J., and Pongratz, J.: Relevance of methodological choices for accounting of land use change carbon fluxes, Global Biogeochemical Cycles, 29, 1230–1246, https://doi.org/10.1002/2014GB004997, 2015.

https://doi.org/10.5194/egusphere-2026-3584
Preprint. Discussion started: 30 June 2026
© Author(s) 2026. CC BY 4.0 License.

Hantson, S., Arneth, A., Harrison, S. P., Kelley, D. I., Prentice, I. C., Rabin, S. S., Archibald, S., Mouillot, F., Arnold, S. R., Artaxo, P., Bachelet, D., Ciais, P., Forrest, M., Friedlingstein, P., Hickler, T., Kaplan, J. O., Kloster, S., Knorr, W., Lasslop, G., Li, F., Mangeon, S., Melton, J. R., Meyn, A., Sitch, S., Spessa, A., van der Werf, G. R., Voulgarakis, A., and Yue, C.: The status and challenge of global fire modelling, Biogeosciences, 13, 3359–3375, https://doi.org/10.5194/bg-13-3359-2016, 2016.

Hantson, S., Kelley, D. I., Arneth, A., Harrison, S. P., Archibald, S., Bachelet, D., Forrest, M., Hickler, T., Lasslop, G., Li, F., Mangeon, S., Melton, J. R., Nieradzik, L., Rabin, S. S., Prentice, I. C., Sheehan, T., Sitch, S., Teckentrup, L., Voulgarakis, A., and Yue, C.: Quantitative assessment of fire and vegetation properties in simulations with fire-enabled vegetation models from the Fire Model Intercomparison Project, Geoscientific Model Development, 13, 3299–3318, https://doi.org/10.5194/gmd-13-3299-2020, 2020.

Harris, I., Osborn, T., Jones, P., and Lister, D.: Version 4 of the CRU TS monthly high-resolution gridded multivariate climate dataset, Scientific Data, 7, https://doi.org/10.1038/s41597-020-0453-3, 2020.

Helbig, M., Daw, L., Iwata, H., Rudaitis, L., Ueyama, M., and Živković, T.: Boreal Forest Fire Causes Daytime Surface Warming During Summer to Exceed Surface Cooling During Winter in North America, AGU Advances, 5, e2024AV001 327, https://doi.org/10.1029/2024AV001327, e2024AV001327 2024AV001327, 2024.

Hoelzemann, J. J., Schultz, M. G., Brasseur, G. P., Granier, C., and Simon, M.: Global Wildland Fire Emission Model (GWEM): Evaluating the use of global area burnt satellite data, Journal of Geophysical Research: Atmospheres, 109, https://doi.org/10.1029/2003JD003666, 2004.

Houghton, R. A. and Castanho, A.: Annual emissions of carbon from land use, land-use change, and forestry from 1850 to 2020, Earth System Science Data, 15, 2025–2054, https://doi.org/10.5194/essd-15-2025-2023, 2023.

Hurtt, G., Chini, L., Frolking, S., Betts, R., Feddema, J., Fischer, G., Fisk, J., Hibbard, K., Houghton, R., Janetos, A., Jones, C., Kindermann, G., Kinoshita, T., Klein Goldewijk, K., Riahi, K., Shevliakova, E., Smith, S., Stehfest, E., Thomson, A., and Wang, Y.: Harmonization of Land-Use Scenarios for the Period 1500-2100: 600 Years of Global Gridded Annual Land-Use Transitions, Wood Harvest, and Resulting Secondary Lands, Climatic Change, 109, 117–161, https://doi.org/10.1007/s10584-011-0153-2, 2011.

Jones, C. and Friedlingstein, P.: Quantifying process-level uncertainty contributions to TCRE and Carbon Budgets for meeting Paris Agreement climate targets, Environmental Research Letters, 15, https://doi.org/10.1088/1748-9326/ab858a, 2020.

Jones, M. W., Veraverbeke, S., Andela, N., Doerr, S. H., Kolden, C., Mataveli, G., Pettinari, M. L., Quéré, C. L., Rosan, T. M., van der Werf, G. R., van Wees, D., and Abatzoglou, J. T.: Global rise in forest fire emissions linked to climate change in the extratropics, Science, 386, eadl5889, https://doi.org/10.1126/science.adl5889, 2024.

Kobayashi, S., Ota, Y., Harada, Y., Ebita, A., Moriya, M., Onoda, H., Onogi, K., Kamahori, H., Kobayashi, C., Endo, H., Miyaoka, K., and Takahashi, K.: The JRA-55 Reanalysis: General Specifications and Basic Characteristics, Journal of the Meteorological Society of Japan, 93, 5–48, https://doi.org/10.2151/jmsj.2015-001, 2015.

Krinner, G., Viovy, N., de Noblet-Ducoudré, N., Ogée, J., Polcher, J., Friedlingstein, P., Ciais, P., Sitch, S., and Prentice, I. C.: A dynamic global vegetation model for studies of the coupled atmosphere-biosphere system, Global Biogeochemical Cycles, 19, https://doi.org/10.1029/2003GB002199, 2005.

Lacroix, F., Liu, M., Ma, M., Resplandy, L., Beusen, A., Hauck, J., Lennartz, S., Li, Y., Tian, H., and Regnier, P.: Biogeochemical river inputs for global ocean models (RivR2O), https://doi.org/10.5281/zenodo.13799103, 2024.

Lizundia-Loiola, J., Otón, G., Ramo, R., and Chuvieco, E.: A spatio-temporal active-fire clustering approach for global burned area mapping at 250m from MODIS data, Remote Sensing of Environment, 236, 111 493, https://doi.org/10.1016/j.rse.2019.111493, 2020.

https://doi.org/10.5194/egusphere-2026-3584
Preprint. Discussion started: 30 June 2026
© Author(s) 2026. CC BY 4.0 License.

Luijkx, I., Peters, W., Lloret, Z., Zhao, M., Niwa, Y., Jacobson, A. R., Liu, J., Byrne, B., Bowman, K., Bloom, A., Jin, Z., Ju, W., Tian, X., Piao, S., Wang, Y., Wang, T., Zhang, H., Rödenbeck, C., Ding, J., Liu, Z., Zeng, N., Feng, L., Jiang, F., Yun, J., Palmer, P., Yang, D., Chandra, N., Chevallier, F., Patra, P., Martinez, A., Nayagam, L., Janardanan, R., and Maksyutov, S.: Global CO2 gridded flux fields from 14 atmospheric inversions in GCB2024, https://doi.org/10.18160/4R5W-VNBV, 2024.

Ma, L., Hurtt, G., Ott, L., Sahajpal, R., Fisk, J., Lamb, R., Tang, H., Flanagan, S., Chini, L., Chatterjee, A., and Sullivan, J.: Global evaluation of the Ecosystem Demography model (ED v3.0), Geoscientific Model Development, 15, 1971–1994, https://doi.org/10.5194/gmd-15-1971-2022, 2022.

Mangeon, S., Voulgarakis, A., Gilham, R., Harper, A., Sitch, S., and Folberth, G.: INFERNO: a fire and emissions scheme for the UK Met Office's Unified Model, Geoscientific Model Development, 9, 2685–2700, https://doi.org/10.5194/gmd-9-2685-2016, 2016.

Moorcroft, P. R., Hurtt, G. C., and Pacala, S. W.: A METHOD FOR SCALING VEGETATION DYNAMICS: THE ECOSYSTEM DEMOGRAPHY MODEL (ED), Ecological Monographs, 71, 557–586, https://doi.org/10.1890/0012-9615(2001)071[0557:AMFSVD]2.0.CO;2, 2001.

Palviainen, M., Laurén, A., Pumpanen, J., Bergeron, Y., Bond-Lamberty, B., Larjavaara, M., Kashian, D. M., Köster, K., Prokushkin, A., Chen, H. Y. H., Seedre, M., Wardle, D. A., Gundale, M. J., Nilsson, M.-C., Wang, C., and Berninger, F.: Decadal-Scale Recovery of Carbon Stocks After Wildfires Throughout the Boreal Forests, Global Biogeochemical Cycles, 34, e2020GB006612, https://doi.org/10.1029/2020GB006612, e2020GB006612 2020GB006612, 2020.

Parker, N. J., Sullins, D. S., Haukos, D. A., Fricke, K. A., and Hagen, C. A.: Recovery of working grasslands following a megafire in the southern mixed-grass prairie, Global Ecology and Conservation, 36, e02 142, https://doi.org/10.1016/j.gecco.2022.e02142, 2022.

Potter, C. S., Randerson, J. T., Field, C. B., Matson, P. A., Vitousek, P. M., Mooney, H. A., and Klooster, S. A.: Terrestrial ecosystem production: A process model based on global satellite and surface data, Global Biogeochemical Cycles, 7, 811–841, https://doi.org/10.1029/93GB02725, 1993.

Poulter, B., Cadule, P., Cheiney, A., Ciais, P., Hodson, E., Peylin, P., Plummer, S., Spessa, A., Saatchi, S., Yue, C., and Zimmermann, N. E.: Sensitivity of global terrestrial carbon cycle dynamics to variability in satellite-observed burned area, Global Biogeochemical Cycles, 29, 207–222, https://doi.org/10.1002/2013GB004655, 2015.

Qin, Z., Zhu, Y., Canadell, J. G., Chen, M., Li, T., Mishra, U., and Yuan, W.: Global spatially explicit carbon emissions from land-use change over the past six decades (1961–2020), One Earth, 7, 835–847, https://doi.org/10.1016/j.oneear.2024.04.002, 2024.

Randerson, J. T., Chen, Y., van der Werf, G. R., Rogers, B. M., and Morton, D. C.: Global burned area and biomass burning emissions from small fires, Journal of Geophysical Research: Biogeosciences, 117, https://doi.org/10.1029/2012JG002128, 2012.

Santín, C., Doerr, S., Preston, C., and González-Rodríguez, G.: Pyrogenic organic matter production from wildfires: A missing sink in the global carbon cycle, Global Change Biology, 21, https://doi.org/10.1111/gcb.12800, 2014.

Sato, L., Gomes, V., Shimabukuro, Y., Keller, M., Arai, E., Dos-Santos, M., Brown, I., and Aragão, L.: Post-Fire Changes in Forest Biomass Retrieved by Airborne LiDAR in Amazonia, Remote Sensing, 8, 839, https://doi.org/10.3390/rs8100839, 2016.

Silva, C., Aragão, L., Barlow, J., Espírito-Santo, F., Young, P., Anderson, L., Berenguer, E., Brasil, I., Brown, F., Castro, B., Farias, R., Ferreira, J., França, F., De Alencastro Graça, P. M., Kirsten, L., Lopes, A., Salimon, C., Scaranello, M., Seixas, M. M., and Xaud, H.: Drought-induced Amazonian wildfires instigate a decadal-scale disruption of forest carbon dynamics, Philosophical Transactions of the Royal Society B: Biological Sciences, 373, 20180 043, https://doi.org/10.1098/rstb.2018.0043, 2018.

Silva, C., Aragão, L., Young, P., Espírito-Santo, F., Berenguer, E., Anderson, L., Brasil, I., Lopes, A., Ferreira, J., Withey, K., França, F., De Alencastro Graça, P. M., Kirsten, L., Xaud, H., Salimon, C., Scaranello, M., Castro, B., Seixas, M. M., Farias, R., and

https://doi.org/10.5194/egusphere-2026-3584
Preprint. Discussion started: 30 June 2026
© Author(s) 2026. CC BY 4.0 License.

Barlow, J.: Estimating the multi-decadal carbon deficit of burned Amazonian forests, Environmental Research Letters, 15, 114 023, https://doi.org/10.1088/1748-9326/abb62c, 2020.

Sitch, S., O'Sullivan, M., Robertson, E., Friedlingstein, P., Albergel, C., Anthoni, P., Arneth, A., Arora, V. K., Bastos, A., Bastrikov, V., Bellouin, N., Canadell, J. G., Chini, L., Ciais, P., Falk, S., Harris, I., Hurtt, G., Ito, A., Jain, A. K., Jones, M. W., Joos, F., Kato, E., Kennedy, D., Klein Goldewijk, K., Kluzek, E., Knauer, J., Lawrence, P. J., Lombardozzi, D., Melton, J. R., Nabel, J. E. M. S., Pan, N., Peylin, P., Pongratz, J., Poulter, B., Rosan, T. M., Sun, Q., Tian, H., Walker, A. P., Weber, U., Yuan, W., Yue, X., and Zaehle, S.: Trends and Drivers of Terrestrial Sources and Sinks of Carbon Dioxide: An Overview of the TRENDY Project, Global Biogeochemical Cycles, 38, e2024GB008 102, https://doi.org/10.1029/2024GB008102, e2024GB008102 2024GB008102, 2024.

Thonicke, K., Venevsky, S., Sitch, S., and Cramer, W.: The role of fire disturbance for global vegetation dynamics: coupling fire into a Dynamic Global Vegetation Model, Global Ecology and Biogeography, 10, 661–677, https://doi.org/10.1046/j.1466-822X.2001.00175.x, 2001.

Thonicke, K., Spessa, A., Prentice, I. C., Harrison, S. P., Dong, L., and Carmona-Moreno, C.: The influence of vegetation, fire spread and fire behaviour on biomass burning and trace gas emissions: results from a process-based model, Biogeosciences, 7, 1991–2011, https://doi.org/10.5194/bg-7-1991-2010, 2010.

Udy, D., Vance, T., Kiem, A., Holbrook, N., and Abram, N.: Australia's 2019/20 Black Summer fire weather exceptionally rare over the last 2000 years, Communications Earth Environment, 5, https://doi.org/10.1038/s43247-024-01470-z, 2024.

van der Werf, G. R., Randerson, J. T., Giglio, L., van Leeuwen, T. T., Chen, Y., Rogers, B. M., Mu, M., van Marle, M. J. E., Morton, D. C., Collatz, G. J., Yokelson, R. J., and Kasibhatla, P. S.: Global fire emissions estimates during 1997–2016, Earth System Science Data, 9, 697–720, https://doi.org/10.5194/essd-9-697-2017, 2017.

van Leeuwen, T. T., van der Werf, G. R., Hoffmann, A. A., Detmers, R. G., Rücker, G., French, N. H. F., Archibald, S., Carvalho Jr., J. A., Cook, G. D., de Groot, W. J., Hély, C., Kasischke, E. S., Kloster, S., McCarty, J. L., Pettinari, M. L., Savadogo, P., Alvarado, E. C., Boschetti, L., Manuri, S., Meyer, C. P., Siegert, F., Trollope, L. A., and Trollope, W. S. W.: Biomass burning fuel consumption rates: a field measurement database, Biogeosciences, 11, 7305–7329, https://doi.org/10.5194/bg-11-7305-2014, 2014.

van Wees, D., van der Werf, G. R., Randerson, J. T., Rogers, B. M., Chen, Y., Veraverbeke, S., Giglio, L., and Morton, D. C.: Global biomass burning fuel consumption and emissions at 500 m spatial resolution based on the Global Fire Emissions Database (GFED), Geoscientific Model Development, 15, 8411–8437, https://doi.org/10.5194/gmd-15-8411-2022, 2022.

Walker, X. J., Rogers, B. M., Baltzer, J. L., Cumming, S. G., Day, N. J., Goetz, S. J., Johnstone, J. F., Schuur, E. A. G., Turetsky, M. R., and Mack, M. C.: Cross-scale controls on carbon emissions from boreal forest megafires, Global Change Biology, 24, 4251–4265, https://doi.org/10.1111/gcb.14287, 2018.

Webb, E. E., Alexander, H. D., Paulson, A. K., Loranty, M. M., DeMarco, J., Talucci, A. C., Spektor, V., Zimov, N., and Lichstein, J. W.: Fire-Induced Carbon Loss and Tree Mortality in Siberian Larch Forests, Geophysical Research Letters, 51, e2023GL105 216, https://doi.org/10.1029/2023GL105216, e2023GL105216 2023GL105216, 2024.

Werf, G., Randerson, J., van Wees, D., Chen, Y., Giglio, L., Hall, J., Vernooij, R., Mu, M., Shahid, S., Barsanti, K., Yokelson, R., and Morton, D.: Landscape fire emissions from the 5 version of the Global Fire Emissions Database (GFED5), Scientific Data, 12, https://doi.org/10.1038/s41597-025-06127-w, 2025.

Xu, L., Saatchi, S. S., Yang, Y., Yu, Y., Pongratz, J., Bloom, A. A., Bowman, K., Worden, J., Liu, J., Yin, Y., Domke, G., McRoberts, R. E., Woodall, C., Nabuurs, G.-J., de Miguel, S., Keller, M., Harris, N., Maxwell, S., and Schimel, D.: Changes in global terrestrial live biomass over the 21st century, Science Advances, 7, eabe9829, https://doi.org/10.1126/sciadv.abe9829, 2021.

https://doi.org/10.5194/egusphere-2026-3584
Preprint. Discussion started: 30 June 2026
© Author(s) 2026. CC BY 4.0 License.

Xu, Y., Zhuang, Q., Zhao, B., Billmire, M., Cook, C., Graham, J., French, N. H., and Prinn, R.: Impacts of wildfires on boreal forest ecosystem carbon dynamics from 1986 to 2020, Environmental Research Letters, 19, 064 023, https://doi.org/10.1088/1748-9326/ad489a, 2024.

Yin, Y., Bloom, A., Worden, J., Saatchi, S., Yang, Y., Williams, M., Liu, J., Jiang, Z., Worden, H., Bowman, K., Frankenberg, C., and Schimel, D.: Fire decline in dry tropical ecosystems enhances decadal land carbon sink, Nature Communications, 11, https://doi.org/10.1038/s41467-020-15852-2, 2020.

Yue, C., Ciais, P., Cadule, P., Thonicke, K., Archibald, S., Poulter, B., Hao, W. M., Hantson, S., Mouillot, F., Friedlingstein, P., Maignan, F., and Viovy, N.: Modelling the role of fires in the terrestrial carbon balance by incorporating SPITFIRE into the global vegetation model ORCHIDEE – Part 1: simulating historical global burned area and fire regimes, Geoscientific Model Development, 7, 2747–2767, https://doi.org/10.5194/gmd-7-2747-2014, 2014.

Zaehle, S., Friend, A., Friedlingstein, P., Dentener, F., Peylin, P., and Schulz, M.: Carbon and nitrogen cycle dynamics in the O-CN land surface model: 2. Role of the nitrogen cycle in the historical terrestrial carbon balance, Global Biogeochemical Cycles, 24, 2010.

Zheng, B., Ciais, P., Chevallier, F., Chuvieco, E., Chen, Y., and Yang, H.: Increasing forest fire emissions despite the decline in global burned area, Science Advances, 7, eabh2646, https://doi.org/10.1126/sciadv.abh2646, 2021.